nature aging

Article

https://doi.org/10.1038/s43587-026-01120-3

Glutamine-driven reductive TCA cycle metabolism supports aged muscle stem cell function via de novo lipogenesis

Received: 22 October 2025

Accepted: 31 March 2026

Published online: 14 May 2026

Check for updates

David E. Lee[1,2,3,4], Lauren K. McKay[1,5,6], Akshay Bareja[1,3], JiaCheng Yang[2], Wentao He[1], Demitrius A. Hill[1], James R. Bain[1,3,4], Shihuan Kuang[2,7,8], Guo-Fang Zhang[1,3], Christopher B. Newgard[1,3,9] & James P. White[1,3,4]

Sarcopenia and the age-related decline in muscular strength and regenerative capacity contribute directly to loss of autonomy, greater risk for hospitalization and healthcare utilization. One contributing cellular phenotype associated with skeletal muscle aging is a loss in the function and number of resident muscle stem cells (MuSCs) or satellite cells. MuSC activation leads to dramatic changes in cellular architecture and metabolic reprogramming, including both mitochondrial biogenesis and increased glycolysis. Despite these changes to increase energy production, high energy demands may not be fully met during periods of MuSC activation. Here we used in vitro and in vivo approaches in mice to demonstrate the function of glutaminase for age-related changes in MuSC function. By combining fluorescence-activated cell sorting (FACS) isolation with metabolomics and stable isotope tracing, we show an age-related decline in reductive (counterclockwise) flux of glutamine through the tricarboxylic acid (TCA) cycle, a pathway by which MuSCs build cellular fatty acid stores as necessary biomass for MuSC function.

Sarcopenia and the age-related decline in muscle strength and regenerative capacity contribute directly to loss of autonomy, greater risk for hospitalization and healthcare utilization[1,2]. Improving resilience could allow for improved mobility and independence. One contributing cellular phenotype associated with skeletal muscle aging is a loss in the function and number of resident MuSCs or satellite cells. MuSCs directly participate in the replacement of myonuclei after muscle injury; however, more recent evidence shows a contribution of MuSCs to myonuclear maintenance even in the absence of damage[3]. The molecular processes governing MuSC quiescence, activation and differentiation to myoblasts have garnered much attention as potential therapeutic targets to enhance muscle resilience. However, the metabolic circuits that support rapid cellular remodeling from a dormant state are not well defined in adult stem cell populations.

Remodeling of the cellular metabolic landscape is a hallmark of stem cell activation[4]. Upon activation by muscle injury or in vitro culture, MuSCs show robust mitochondrial biogenesis and increased capacity for mitochondrial oxygen consumption[5,6]. The energetic demands required for cellular remodeling from quiescence to a rapidly replicating state are thought to drive an increase in mitochondrial

[1]Sarah W. Stedman Nutrition and Metabolism Center and Duke Molecular Physiology Institute, Duke University School of Medicine, Durham, NC, USA. [2]Department of Orthopaedic Surgery, Duke University School of Medicine, Durham, NC, USA. [3]Department of Medicine, Duke University School of Medicine, Durham, NC, USA. [4]Duke Center for the Study of Aging and Human Development, Duke University School of Medicine, Durham, NC, USA. [5]Department of Oral and Craniofacial Molecular Biology, Virginia Commonwealth University, Richmond, VA, USA. [6]Department of Biomedical Sciences, Adams School of Dentistry, University of North Carolina at Chapel Hill, Chapel Hill, NC, USA. [7]Department of Pathology, Duke University School of Medicine, Durham, NC, USA. [8]Department of Cell Biology, Duke University School of Medicine, Durham, NC, USA. [9]Department of Pharmacology and Cancer Biology, Duke University School of Medicine, Durham, NC, USA. e-mail: james.white@duke.edu

energy production. However, activated MuSCs also upregulate glycolysis, suggesting that oxidative phosphorylation may not be fully meeting the energy demands of the cell[5,7]. Consistent with an overall energy deficit, phosphorylation of AMPK is increased in activated stem cells despite greater glycolytic and mitochondrial energy production[6,8,9]. This suggests that changes in metabolism during MuSC activation may not be directly related to ATP production. Ryall et al.[7] provided evidence to support this concept by showing that increased glycolytic flux supports cytoplasmic acetyl-CoA production used in protein acetylation during MuSC differentiation. Glutamine is a versatile metabolic substrate that can be used in pathways related to conversion to other amino acids, synthesis of nucleic acids and energy production[10]. Other stem cell populations, including skeletal stem cells, have been shown to be reliant on glutamine metabolism for proliferation and bone formation[11]. Recent data from Soro-Arnáiz et al.[12] demonstrate greater anaplerotic metabolism of glutamine in proliferating myoblasts compared to differentiated myotubes. Moreover, some rapidly dividing or differentiating cells, including cancer cells, use a glutamine-dependent reductive carboxylation pathway to form citrate for processes such as de novo lipogenesis (DNL)[13]. The reliance of glutamine metabolism, and, more specifically, the utility of the reductive carboxylation and downstream biosynthetic pathways, has not been investigated in the MuSC in the context of stem cell aging.

A holistic understanding of metabolic remodeling in response to stem cell activation, and how such responses become impaired with aging, is needed to better understand how to revive stem cells in aging muscle. In this study, we used targeted metabolomics and flux analysis datasets to identify a crucial metabolic pathway for MuSC activation: glutamine metabolism. Using in vitro and in vivo approaches, we demonstrate the function of glutaminase (GLS) for age-related changes to MuSC function. By combining FACS isolation with stable isotope tracing, we identify an age-related decline in reductive, counterclockwise flux of glutamine through the TCA cycle to form citrate and contribute to DNL, thereby providing lipids needed for rapid cellular growth and replication.

Results

GLS supports MuSC metabolism for successful activation in vitro

We tested the necessity of pyruvate, fatty acids and glutamine for MuSC activation by monitoring incorporation of 5-ethynyl-2′-deoxyuridine (EdU) in freshly isolated MuSCs (Supplementary Fig. 1) with specific inhibitors for each fuel substrate (Fig. 1a,b and Supplementary Fig. 2a–c). Although there was reduced EdU incorporation observed with inhibition of pyruvate and fatty acid metabolism at the 24-hour timepoint, these groups regained proliferative rates similar to control MuSCs at the 48-hour and 72-hour timepoints (Fig. 1a,b). By contrast, only MuSCs treated with the GLS inhibitor BPTES had a marked reduction in proliferation throughout all timepoints (Fig. 1a,b). To assess whether GLS inhibition would affect MuSC survival, we measured apoptosis in vitro via terminal deoxynucleotidyl transferase dUTP nick end labeling (TUNEL). We found a 30% increase in TUNEL staining ($P < 0.001$) in BPTES-treated MuSCs compared to vehicle (Fig. 1c,d).

To better understand the changes in MuSC activation during GLS inhibition, we performed ex vivo experiments using intact myofibers (Fig. 1e,f). Seventy-two hours after myofiber isolation, BPTES-treated myofibers had 45% fewer PAX7$^+$Ki67$^+$ nuclei compared to vehicle control ($P< 0.001$; Fig. 1e,f), once again suggesting a reduced proliferative rate with GLS inhibition. Because treatment with BPTES directly prevents glutamine anaplerosis, we tested the oxygen consumption rate (OCR) of control and BPTES-treated MuSCs. At all timepoints, basal OCR was significantly reduced in BPTES-treated wells (by 33%, $P = 0.038$); however, these differences were lost upon injection of the electron transport inhibitor oligomycin and ATP synthase inhibitor rotenone/antimycin A, suggesting that the differences in OCR were directly linked to substrate oxidation (Fig. 1g). For a more global view of the metabolic landscape of the activating MuSCs (beyond just extracellular measurements of OCR), we performed non-targeted metabolomic phenotyping to characterize the GLS-supported metabolic signature in MuSCs. For this experiment, we analyzed two groups of MuSCs that were isolated and cultured in vitro for 24 hours with a 1-hour treatment period by either vehicle (control) or BPTES before collecting metabolite extracts for ultra-high-performance liquid chromatography–mass spectrometry (UHPLC–MS) metabolomics. The lack of GLS activity (confirmed by glutamine and glutamate abundances) resulted in deficiencies in several metabolic intermediates across multiple metabolic pathways, including a significant reduction in ATP level and increase in AMP levels (Fig. 1h). These initial results support a critical role for the glutamine pathway in MuSC proliferation, survival and metabolism.

GLS is supportive of successful MuSC activation in vivo

Because experiments in Fig. 1 show a clear in vitro phenotype of GLS inhibition and glutamine deprivation in isolated MuSCs, we next sought to determine the contribution of GLS function to MuSC activation in an in vivo regenerative context. We generated a MuSC-specific, inducible *glutaminase1* knockout mouse line by crossbreeding *Pax7*-CreER^{T2} (Gaka strain) mice with a *Gls*$^{fl/fl}$ mouse strain[11] to allow tamoxifen-inducible, MuSC-specific depletion of the *Gls1* gene (Pax7$^{Gls-/-}$; Fig. 2a; see Methods for specific strain details). Pax7$^{Gls-/-}$ mice were treated with tamoxifen no earlier than 4 months of age to ensure full development. Fourteen days after tamoxifen administration (or corn oil for controls), MuSCs were isolated from uninjured muscle for immunoblot analysis of GLS1, demonstrating a 53% reduction in GLS1 protein abundance ($P < 0.001$; Fig. 2b). Flow cytometry analysis of isolated MuSCs shows a decline in the percent of MuSCs from uninjured muscles (approximately 0.8% lower VCAM1$^+$ cells, 8% relative reduction, in percentage of VCAM1$^+$ cells to non-heme cells, $P = 0.061$; Fig. 2c) as well as a blunted response to barium chloride ($BaCl_2$) injury in the tibialis anterior muscle (25% reduction in MuSCs relative to non-heme cells, $P = 0.015$; Fig. 2d). To substantiate the flow cytometry analysis, we performed immunofluorescence of PAX7 on muscle sections from uninjured and 4 days post-$BaCl_2$ muscles. Quantification of the PAX7$^+$ nuclei showed no differences in quiescent (subsarcolemmal) satellite cells in the uninjured state, although this was only 2 weeks after GLS ablation ($P = 0.174$; Fig. 2e,f). However, once activated by $BaCl_2$ injection, the increased number of PAX7$^+$ cells at the 4-day timepoint was ablated in the tamoxifen-treated Pax7$^{Gls-/-}$ muscles ($P = 0.038$; Fig. 2g,h). Using the same experimental design, we collected the tibialis anterior muscles 4 days after $BaCl_2$ for histological analysis of embryonic myosin heavy chain (eMHC), a marker of early muscle regeneration (Fig. 2i). Tamoxifen-treated Pax7$^{Gls-/-}$ mice showed significantly reduced fluorescence of eMHC, and regenerating fibers were 19% smaller ($P = 0.039$; Fig. 2j,k). Next, we used a 14-day recovery timepoint after $BaCl_2$ treatment in the tibialis anterior to determine the degree of regeneration between groups (Fig. 2l). Analysis of hematoxylin and eosin (H&E) staining showed a reduction in tibialis anterior muscle fiber cross-sectional area (CSA) by 29.2% in tamoxifen-treated Pax7$^{Gls-/-}$ mice compared to tibialis anterior from vehicle-treated controls ($P = 0.032$; Fig. 2m,n). Finally, we reanalyzed the 14-day injury timepoint to determine the proportion of PAX7$^+$ cells that were interstitial or subsarcolemma during the resolution of regeneration (Fig. 2o). Similar to findings at the earlier timepoint, we saw that tamoxifen-treated mice had a reduction in the total number of PAX7$^+$ cells (Fig. 2p; $P < 0.001$), and the proportion of those subsarcolemmal PAX7$^+$ cells was also reduced (Fig. 2q; $P = 0.024$). Although our experiments do not include tamoxifen-treated Cre$^-$ controls, evidence suggests minimal *Pax7*-CreER^{T2}-driven regeneration defects in the strain used here (see mouse strain details in Methods)[14]. These results further support the necessity for GLS in the MuSCs during muscle injury.

https://doi.org/10.1038/s43587-026-01120-3

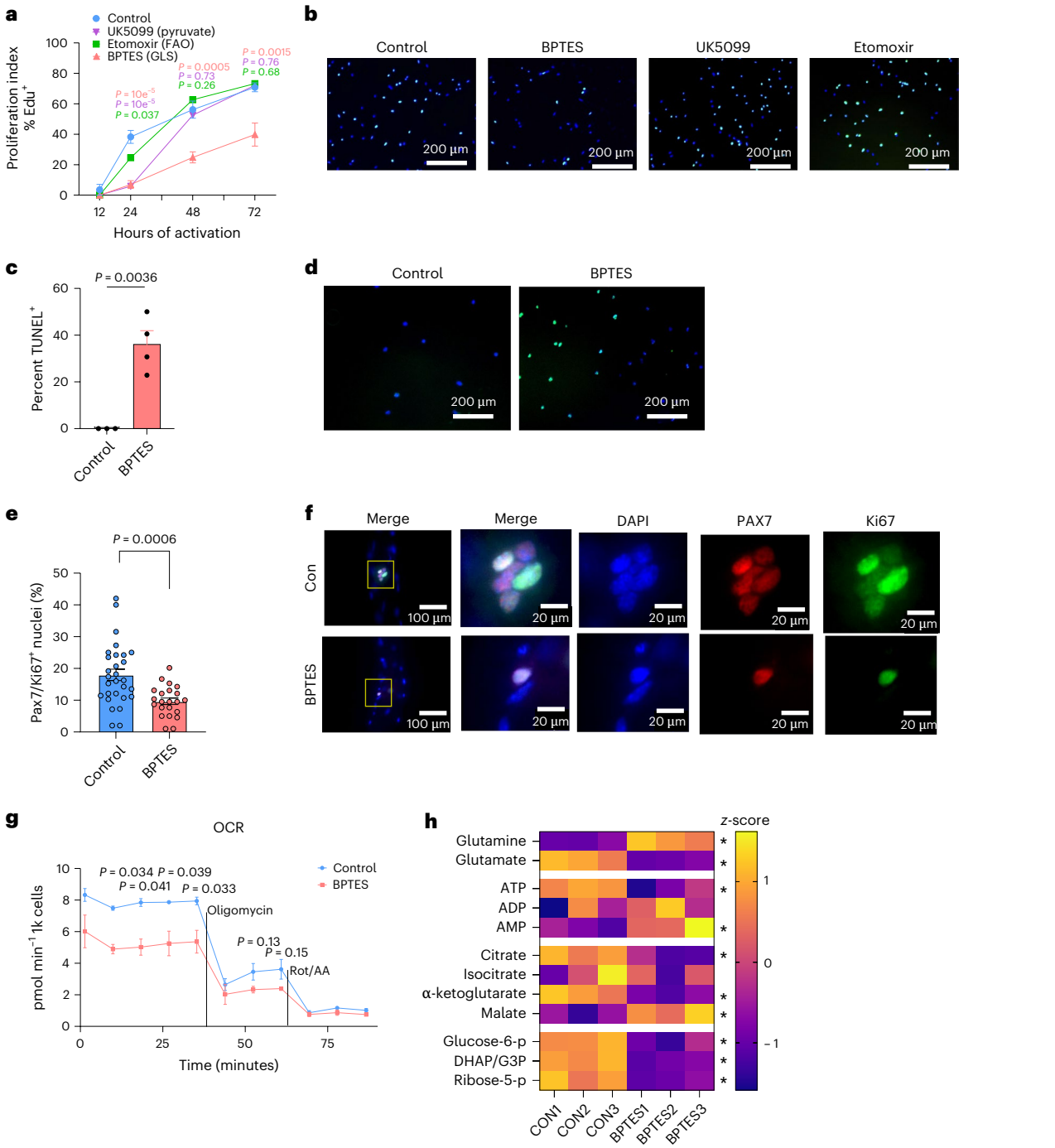


Fig. 1 | MuSCs require glutamine for successful activation in vitro. a, EdU was added to freshly isolated MuSCs to measure rate of activation as a percent of EdU$^+$ cells to total nuclei over time in vehicle-treated (control), 1 µM BPTES-treated (GLS), 3 µM etomoxir-treated (fatty acid oxidation) and 2 µM UK5099-treated (pyruvate) conditions ($n = 9$ per group per timepoint biological replicates; data are mean ± s.e.m.; two-sided t-test was used to compare each treatment to control at each timepoint, without correction for multiple comparisons). **b**, Representative micrographs of EdU (green) and DAPI (blue) at 48-hour timepoint. **c**, Quantified TUNEL assay of MuSCs 48 hours after isolation—results shown are TUNEL$^+$ cells as a percent of total nuclei ($n = 3$ (control) and $n = 4$ (BPTES) biological replicates; data are mean ± s.e.m.; P value indicates two-tailed Student's t-test). **d**, Representative micrographs of TUNEL (green) and DAPI (blue) from **c**. **e**, Individual myofibers were isolated and cultured for 72 hours before fixation and immunostaining of PAX7 and Ki67 to analyze MuSC proliferation in situ. Each point represents an individual isolated fiber ($n = 29$ control, $n = 22$ BPTES; data are mean ± s.e.m.; P value indicates two-tailed t-test). **f**, Representative micrographs of **e**. **g**, Isolated MuSCs were cultured for 48 hours on Seahorse XFe 24-well plates and analyzed by Seahorse Extracellular Flux Analysis. OCRs were normalized to total cell number (quantified immediately after analysis) ($n = 3$ biological replicates per group; data are mean ± s.e.m.; P value indicates two-tailed t-test at specified timepoint without correction for multiple comparisons). **h**, MuSCs were activated in vitro for 24 hours before 1-hour treatment with BPTES and subsequent extraction for untargeted metabolomics by LC–MS. Abundances were $\log_2$ transformed and z-scaled ($n = 3$ per group; asterisk represents $P < 0.05$, Student's two-tailed t-test). 1k, 1,000; FAO, fatty acid oxidation; Rot/AA, rotenone/antimycin A.

GLS is deficient in old MuSCs but sufficient to enhance MuSC transplantation

Many of our findings observed with GLS loss of function in MuSCs (altered metabolism, activation and regeneration) are reminiscent of deficiencies seen in the context of aged MuSCs. We first wanted to determine if aged MuSCs had altered expression of GLS. We measured protein expression of GLS in FACS-isolated MuSCs from uninjured mouse muscle (Fig. 3a) and found a significant 51% reduction in GLS abundance in MuSCs from 24-month (old) compared to 6-month (young) samples (Fig. 3b and Supplementary Fig. 3a; $P = 0.007$). We queried a publicly available single-cell RNA sequencing dataset recently made available by Lai et al.[15], which showed a similar downregulation of the *Gls1* transcript in aged human donors compared to young (Supplementary Fig. 3b). We then isolated MuSCs from the two age groups and analyzed proliferation by incorporation of EdU during the initial phase of MuSC in vitro activation in the presence and absence of the GLS inhibitor BPTES. Aged MuSCs had an inherent reduction in proliferation (14%, $P < 0.001$) 48 hours after isolation compared to young MuSCs. Proliferation was decreased by an additional 40% when old MuSCs were treated with BPTES ($P < 0.001$; Fig. 3c). A similar pattern of results was seen when we analyzed young and old MuSC OCR. Old MuSCs had 48% lower basal OCR compared to young MuSCs ($P < 0.001$), which was further lowered in old MuSCs treated with BPTES (68% lower in old BPTES versus old, $P = 0.005$; Fig. 3d). Based on our observation of decreased EdU incorporation and OCR in BPTES-treated old MuSCs compared to old controls, we hypothesized that residual, but reduced, GLS activity continues to contribute to the activation of old MuSCs and that increasing GLS expression might enhance old MuSC function. To test this hypothesis, we performed a transplantation experiment using lentiviral-driven expression of GLS1 in MuSCs from 24-month-old mice (Fig. 3e). We validated reporter expression, GLS protein abundance and GLS conversion of glutamine to glutamate in MuSCs transduced with lenti-gls (Fig. 3f and Supplementary Fig. 4a–e). We transplanted these MuSCs (from 24-month-old donor mice) into the tibialis anterior muscle of 24-month-old recipients 1 day after $BaCl_2$ injection, using one limb for lenti-gfp cells and the contralateral limb for lenti-gls cells. Thirteen days after transplantation, we excised tibialis anterior muscle and performed immunofluorescence using anti-GFP and anti-PAX7 antibodies to assess contribution of donor cells toward regenerating myofibers and the remaining $PAX7^+$ stem cell pool (Fig. 3g). We found a significantly greater proportion of regenerated fibers as GFP^+ in the lenti-gls-treated tibialis anterior muscle (73% greater, $P = 0.002$; Fig. 3h), and those GFP^+ fibers in the lenti-gls limb were larger than the GFP^+ fibers in the lenti-gfp transplanted limb (mean difference of 422 μm^2; Fig. 3i,j). When we counted the proportion of $PAX7^+GFP^+$ nuclei, we did not see a difference in the number of GFP-labeled donor cells replenishing the $PAX7^+$ quiescent pool. These results indicate that, in the pathological context of aging, GLS is deficient in the aged MuSC yet still supportive for activation and metabolism. Moreover, the restoration of GLS1 expression is a potential therapeutic target to enhance myogenic function in aged MuSCs.

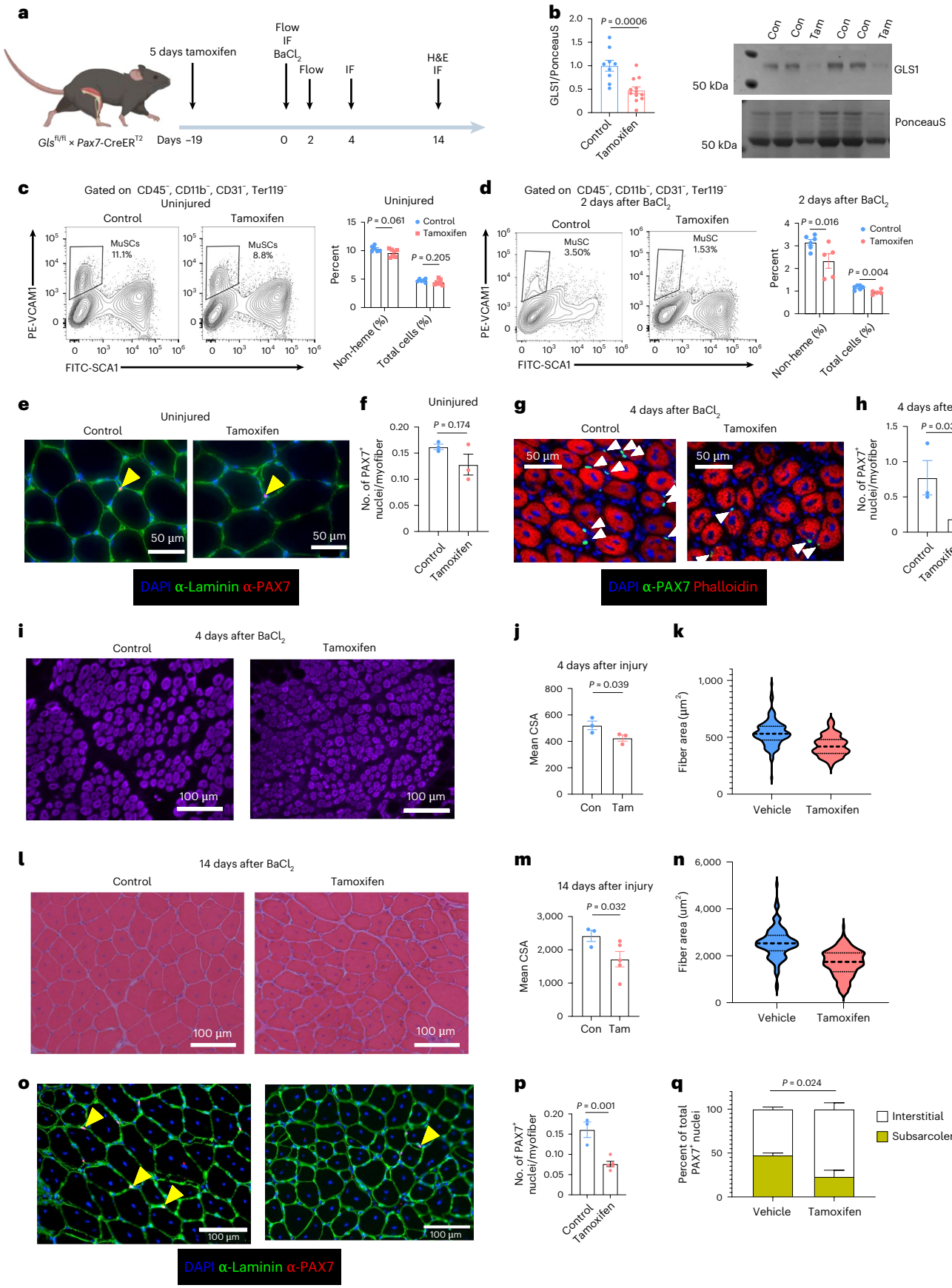
Stable isotope flux analysis of glutamine during aged MuSC activation

To directly assess the utilization of glutamine in the TCA cycle, we activated FACS-isolated MuSCs for 24 hours followed by incubation with 200 µM [$^{13}C_5$] glutamine. After 2 hours of incubation, cell extracts were prepared in ice-cold methanol and subjected to gas chromatography–mass spectrometry (GC–MS) analysis of ^{13}C-labeled mass isotopomers of glutamine-derived metabolites (for example, M0, M1, …M_n ^{13}C-labeled carbons) (Fig. 4a). We verified that the cellular glutamine pool consisted entirely of M5-glutamine in both old and young MuSCs (Fig. 4b). Glutamate and α-ketoglutarate were effectively labeled as well, with predominance of the M5 isotopomer, but labeling of both of these metabolites was reduced in MuSCs from 24-month-old mice compared to 6-month-old young mice (Fig. 4c,d; $P = 0.009$ and $P = 0.018$, respectively), consistent with the lower levels of GLS activity in aged MuSCs. Citrate can be derived from glutamine by M4 oxaloacetate and/or M2 acetyl-CoA (generated through pyruvate anaplerosis) to generate M2, M4 or M6 isotopomers of citrate (Fig. 4a, orange box). All of these labeled species of citrate were present at higher levels in young compared to old MuSCs (Fig. 4e). Interestingly, we also saw clear labeling of M5 citrate, which is generated by the reductive TCA cycle metabolism involving isocitrate dehydrogenase 2 (IDH2) (Fig. 4a, purple box)[16]. We found that M5 citrate was reduced by approximately 80% in old compared to young MuSCs ($P < 0.001$; Fig. 4e). Taken together, these data demonstrate reduced glutamine metabolism through the TCA cycle in aged MuSCs with a clear decrease in oxidative metabolism (reflected in decreases in M2, M4 and M6 citrate), which is accompanied by a proportionate decrease in reductive flux of glutamine (reflected in decreased M5 citrate). Similar levels of reductive carboxylation of glutamine to citrate by proliferating MuSCs was recently published by Soro-Arnáiz et al.[12]; however, the downstream consequences of this process and the impact of age-related MuSC function have yet to be explored, so we chose to investigate reductive MuSC glutamine metabolism.

We next wanted to determine if restoring Gls1 expression in aged MuSCs would enhance energy production and if concurrent inhibition of the reductive glutamine pathway would negate such benefits. To test this, we measured OCR from 6-month (young) and 24-month (old) MuSCs at 48 hours after FACS isolation. During the first 24 hours, we transduced a group of old MuSCs with a lentiviral-Gls1 vector to overexpress GLS (old Gls) and subsequently treated the cells with 10 µM AGI6780, a selective IDH2 inhibitor[16]. Basal OCR was 16% lower in old MuSCs compared to young (Fig. 4f; $P = 0.019$) but was restored to the level of young MuSCs upon overexpression of *Gls1* ($P = 0.009$ old versus old *Gls1*). Interestingly, old MuSCs treated with the IDH2 inhibitor AGI6780 exhibited a further 21% induction of basal OCR ($P = 0.045$) and maintained high levels of oxygen consumption after oligomycin treatment (Fig. 4f). To understand the connection between energy production (OCR) and MuSC activation, we measured in vitro EdU incorporation in the same treatment groups throughout 72 hours in culture. The first 24 hours were used to transduce either lentiviral-*Gfp* (control) or lentiviral-*Gls* before addition of EdU and fixation during

Fig. 2 | MuSC GLS is required for successful activation and regeneration in vivo. a, *Pax7*-CreER^{T2}×*Gls*$^{fl/fl}$ mice were bred to produce $Pax7^{Gls-/-}$ experimental cohorts where mice received either corn oil vehicle (Con) or tamoxifen (Tam) for 5 days. Two weeks after the final Tam dose, mice were used for experiments. **b**, Immunoblot analysis of GLS1 to validate genetic model. Protein was isolated from FACS-isolated MuSCs ($n = 9$ Con, $n = 12$ Tam biological replicates; data are mean ± s.e.m.). **c**,**d**, Flow cytometry of MuSCs from $Pax7^{Gls-/-}$ uninjured limb muscles, $n = 6$ per group, data are mean ± s.e.m. (**c**); or 2-day $BaCl_2$-injected tibialis anterior, $n = 5$ per group, data are mean ± s.e.m. (**d**). **e**–**h**, Immunofluorescence staining by anti-PAX7 antibody (**e**,**g**) and quantification of $PAX7^+$ nuclei in uninjured (**f**,**h**), $n = 3$ biological replicates per group, data are mean ± s.e.m. (**e**,**f**); and 4 days after $BaCl_2$, $n = 3$ biological replicates per group, data are mean ± s.e.m. (**g**,**h**) tibialis anterior muscles from Con or Tam-treated $Pax7^{Gls-/-}$. White arrowheads in **g** indicate $PAX7^+$ nuclei. **i**, eMHC immunofluorescence of 4-day $BaCl_2$-injected tibialis anterior muscles from $Pax7^{Gls-/-}$. Mean CSA (data are mean ± s.e.m.) (**j**) and fiber size frequency distribution from eMHC 5-day histology (**k**), $n = 3$ biological replicates per group; center dashed line is mean; thin dotted lines are upper and lower quartile bounds. **l**, Fourteen days after $BaCl_2$-injected tibialis anterior histology by H&E staining. Mean CSA ($n = 3$ Con, $n = 5$ Tam; data are mean ± s.e.m.) (**m**) and fiber size distribution ($n = 3$ Con, $n =$ Tam) (**n**); center dashed line is mean; thin dotted lines are upper and lower quartile bounds). **o**, PAX7 and laminin immunofluorescence of 14-DPI tibialis anterior with $PAX7^+$ cells per myofiber quantified in **p** ($n = 3$ Con, $n = 5$ Tam; data are mean ± s.e.m.) and proportion of subsarcolemmal PAX7 cells in **q** ($n = 3$ Con, $n = 5$ Tam; data are mean ± s.e.m.). Yellow arrowheads indicate $PAX7^+$ nuclei under basal lamina. *P* values indicate two-tailed *t*-test. Con, control; DPI, days post injection; IF, immunofluorescence. Graphic in **a** created in BioRender; Lee, D. https://biorender.com/5jy97i9 (2026).

https://doi.org/10.1038/s43587-026-01120-3



https://doi.org/10.1038/s43587-026-01120-3

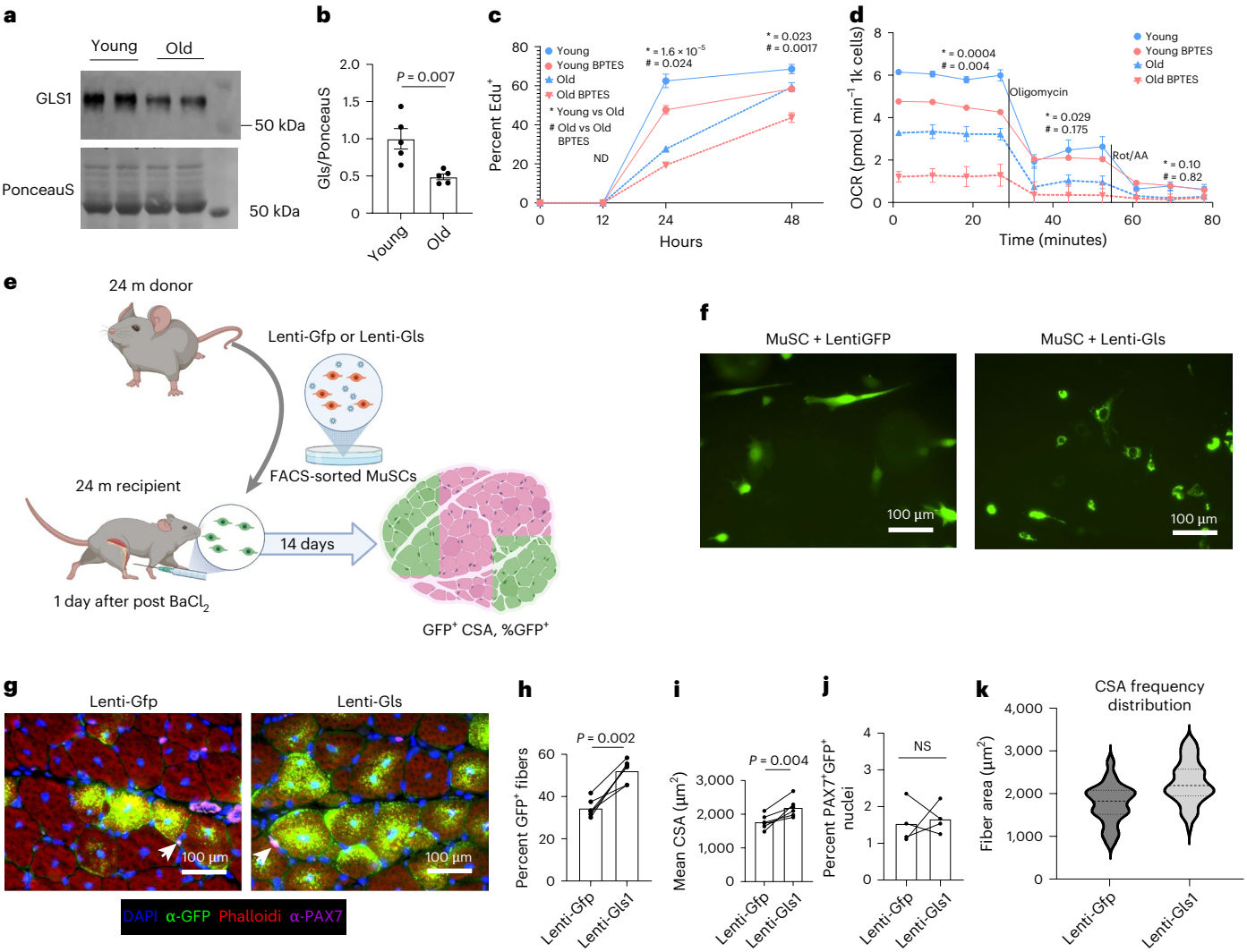


Fig. 3 | GLS is deficient in old MuSCs and is sufficient to enhance MuSC transplantation. a,**b**, Freshly isolated MuSCs were used for immunoblot analysis of GLS1 from C57/B6 young (6 months) or old (24 months) limb muscles ($n = 5$ biological replicates per group; data are mean ± s.e.m.; P represents two-tailed t-test). **c**,**d**, EdU incorporation assay of MuSC activation ($n = 3$ per group per timepoint; data are mean ± s.e.m.) (**c**) and Seahorse OCR analysis ($n = 3$ biological replicates per group; data are mean ± s.e.m.) from young (6 months) or old (24 months) (**d**) under control media or with 1 µM BPTES to inhibit GLS activity. P indicates two-tailed t-test between indicated groups. **e**, Experimental design of transplantation studies. Donor MuSCs were isolated from 24-month-old mice, transfected ex vivo with lentivirus-GFP control or lentivirus-GFP-Gls1 for 24 hours before being injected into recipient (24-month-old, 1 day after $BaCl_2$ injection) tibialis anterior muscles. Recipient mice received lenti-gls MuSCs in one tibialis anterior, and contralateral limb received lenti-control MuSCs ($n = 6$ recipient mice). **f**, Micrographs of MuSC lentiviral GFP reporter expression in vitro; representative micrograph from five repeated experiments. **g**, Immunofluorescence staining with anti-PAX7 and anti-GFP antibodies in transplanted muscle sections from 14 days after $BaCl_2$ injection (13 days after transplant) with DAPI and phalloidin staining of nuclei and actin, respectively ($n = 3$ mice). White arrows indicate $PAX7^+$ and GFP^+ nuclei. **h**, Percent engraftment (GFP fibers/total fibers) ($n = 6$ per group; data are mean ± s.e.m.). **i**, Average CSA of GFP^+ fibers ($n = 6$ per group; data are mean ± s.e.m.). Percent $PAX7^+GFP^+$ nuclei ($n = 4$ per group; data are mean ± s.e.m.) (**j**) and CSA fiber distribution of GFP^+ fibers ($n = 3$ per group, >30 fibers per sample; center dashed line is mean; thin dotted lines are upper and lower quartile bounds) (**k**). P values indicate one-tailed t-tests. Connected data points in **h**–**j** are contralateral-matched samples from the same mouse. 1k, 1,000; m, month; NS, not significant; Rot/AA, rotenone/antimycin A. Graphic in **e** created in BioRender; Lee, D. https://biorender.com/5jy97i9 (2026).

the subsequent 48 hours (Fig. 4g). We again observed a greater rate of EdU incorporation in young MuSCs compared to old ($P < 0.001$ at each timepoint; Fig. 4g). Matching the OCR data, the old *Gls*-lenti MuSCs activated as rapidly as the young and had 36–43% more EdU^+ cells than old MuSCs treated with the control *Gfp*-lenti ($P < 0.001$ at each timepoint; Fig. 4g). Although the *Gls*-lenti treatment improved EdU incorporation throughout the 48-hour labeling period, concurrent treatment with AGI6780 prevented the rescuing effects and reduced proliferation by 32% ($P < 0.001$; Fig. 4g), returning proliferation levels back to old MuSCs. Notably, the effects of the AGI6780 were not due to drug toxicity at the selected doses (Supplementary Fig. 5), and the drug's inhibitory effects on metabolism were specific to reductive IDH2 inhibition (Supplementary Fig. 6a). Together, these results show that forced expression of GLS1 in aged MuSCs can restore proliferation and metabolism, which is dependent on the reductive glutamine pathway.

IDH2 is required by MuSCs to support cellular fatty acid levels during activation

Although our data highlight the importance of the reductive glutamine pathway in the MuSC, the metabolic pathways and cellular function supported by reductive flux in MuSCs remain undefined. We hypothesized that reductive glutamine flux (via IDH2) may serve to generate

https://doi.org/10.1038/s43587-026-01120-3

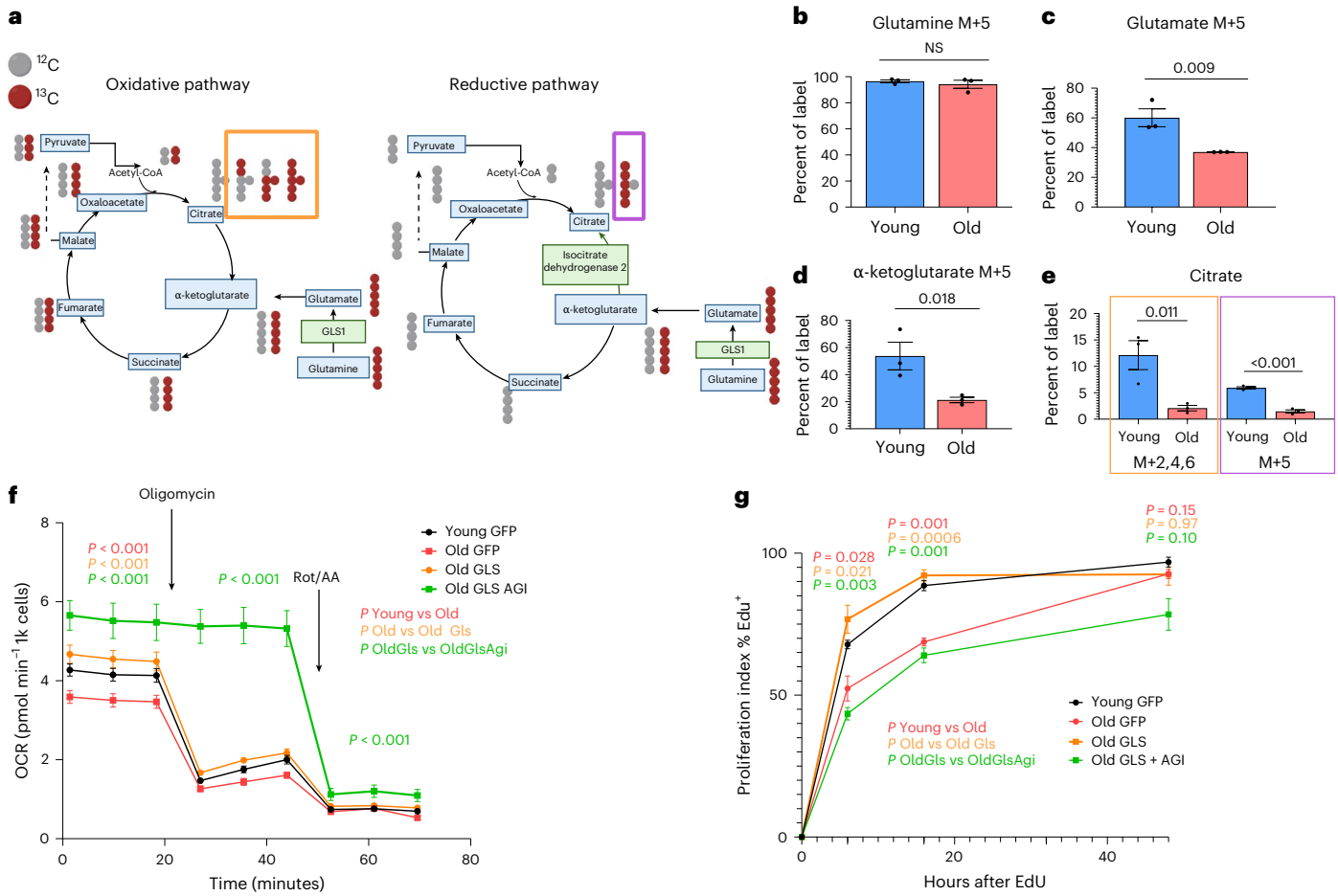


Fig. 4 | Aged MuSCs have proportionately lower reductive glutamine flux during activation. a, Schematic of labeling strategy with U-$^{13}C_5$-glutamine through the TCA cycle with possible oxidative labeling of citrate in the orange box and possible reductive labeling of citrate in the purple box. **b**–**e**, Resulting labeling percentage of indicated isotopomers for glutamine M + 5 (**b**), glutamate M + 5 (**c**), α-ketoglutarate M + 5 (**d**) and oxidative and reductive citrate isotopomers (**e**) ($n = 3$ biological replicates per group; data are mean ± s.e.m.). **f**,**g**, Seahorse OCR analysis ($n = 3$ biological replicates per group (**f**) and EdU incorporation of in vitro activating MuSCs with treatment of AGI6780 to inhibit IDH2 reductive TCA flux; $n = 3$ biological replicates per group per timepoint (**g**); data are mean ± s.e.m.; *P* values indicate two-tailed *t*-tests.). 1k, 1,000; NS, not significant; Rot/AA, rotenone/antimycin A. Graphic in **b** created in BioRender; Lee, D. https://biorender.com/5jy97i9 (2026).

biomolecules needed for cell transformation and division during the initial phase of activation from quiescence. To test this hypothesis, we isolated MuSCs from 6-month-old mice, cultured them in the presence or absence of the selective IDH2 inhibitor AGI6780 for 24 hours and performed targeted metabolomics analyses on fatty acids (Fig. 5a), amino acids (Fig. 5b) and nucleotides (Fig. 5c). AGI6780-treated cells had significantly lower levels of several common fatty acids (C6, C8, C10, C12 and C16 fatty acids by approximately 1.5 s.d., $P = 0.05$; Fig. 5d). Nucleotide abundances shifted from an energized state (more nucleotide triphosphates) to a less energetic state (increased diphosphates and monophosphates) when treated with AGI6780, although total nucleotide levels remained unchanged ($P = 0.45$; Fig. 5c,d). These shifts in the metabolite abundances were accompanied by a doubling of basal OCR in AGI6780-treated MuSCs compared to controls ($P < 0.001$; Fig. 5e) and a resistance to oligomycin-induced decrease in oxygen consumption, similar to what was observed in Fig. 4i. We hypothesized that IDH2 inhibition was forcing glutamine oxidation in the TCA cycle, which accounted for greater basal OCRs and reductions in fatty acid levels by reducing citrate-supported DNL (Fig. 5f). To directly monitor the extent to which reductive glutamine flux supports DNL in MuSCs, we used deuterated water (D_2O) to label palmitate synthesis (Fig. 5g,h)[8]. In MuSCs isolated from 6-month-old mice, we observed a 15% decrease in DNL in AGI6780-treated MuSCs versus vehicle-treated matched controls ($P = 0.013$; Fig. 5h). To test this in vivo, we performed a MuSC transplantation study using a young whole body GFP mouse (6 months old) where we isolated MuSCs (Supplementary Fig. 7) before treatment with an inhibitor of fatty acid synthetase (GSK2194069, termed FASNi) to determine the necessity for this pathway to support MuSC activation (Fig. 5i and Supplementary Fig. 6b). We used anti-GFP immunofluorescence of muscle sections taken 14 days after injury and observed decreases in fiber size and engraftment in FASNi-treated MuSC donors (Fig. 5j–l). These data suggest that glutamine reductive metabolism supports MuSC DNL and energy metabolism. Furthermore, inhibition of the downstream lipogenic pathway in young MuSCs reduces myogenic function.

Reductive glutamine flux supports MuSC activation via DNL

With the findings that reductive glutamine flux through IDH2 supports DNL, we hypothesized that reduced function of aged MuSCs could be rejuvenated by replacing the fatty acid end products of reductive glutamine flux. Measuring in vitro proliferation via Edu incorporation, we overexpressed *Gls1* in old MuSCs in combination with AGI6780 to inhibit IDH2. We also included treatment with the dietary lipids palmitate and oleate as a cell-permeable end product of DNL. We used a combination of palmitate with oleate because it offers a better approximation of physiological lipid conditions as published by our group[17,18]. Similar

https://doi.org/10.1038/s43587-026-01120-3

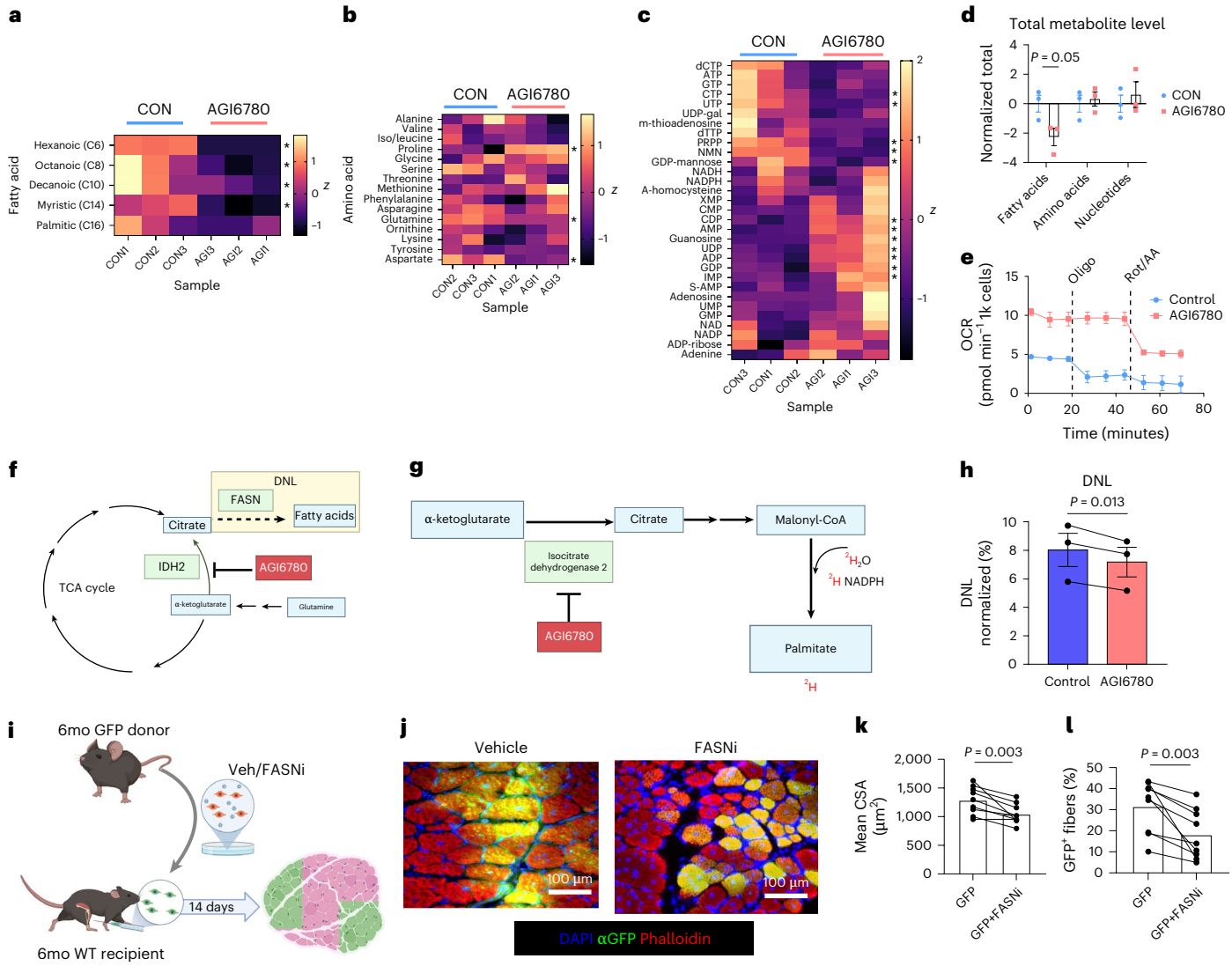


Fig. 5 | IDH2 supports reductive glutamine metabolism to support cellular fatty acid pool. Metabolomics analysis of 6-month-old MuSCs activated for 24 hours in vitro treated with IDH2 inhibitor AGI6780 ($n = 3$ biological replicates per group; data are mean ± s.e.m.: fatty acids (**a**), amino acids (**b**), nucleotides (**c**) and combined total levels of each metabolite category normalized to control (**d**)). Asterisk indicates $P < 0.05$, Student's one-tailed t-test. **e**, Seahorse OCR analysis of 6-month MuSCs treated with AGI6780 during activation in vitro ($n = 3$ biological replicates per group; data are mean ± s.e.m.). **f**, Conceptual illustration of reductive glutamine flux influencing both OCRs and fatty acid abundances. **g**, Schematic diagram of deuterium labeling of palmitate to directly assess DNL. **h**, Percent DNL in isolated MuSCs from 6-month-old mice treated with vehicle or AGI6780 ($n = 3$ per group; data are mean ± s.e.m.). **i**–**l**, Experimental design (**i**), anti-GFP immunofluorescence micrographs (**j**) and quantification of MuSC transplant experiment in 6-month young mice using MuSCs treated with the fatty acid synthase inhibitor GSK2194069 (FASNi) (**k**,**l**) ($n = 9$ recipient mice; data are mean ± s.e.m.). Connected datapoints from **h**, **k** and **l** are contralateral-matched samples from the same mouse. P values indicate two-tailed t-tests. 1k, 1,000; mo, month; Veh, vehicle; Rot/AA, rotenone/antimycin A; WT, wild-type. Graphics in **f** and **g** created in BioRender; Lee, D. https://biorender.com/5jy97i9 (2026).

to our previous experiments (Fig. 4j), old MuSCs with lentiviral-driven GLS expression had reduced activation when treated with AGI6780 (by 18–31%, $P < 0.001$), which was restored to the level of the controls when media were supplemented with 200 µM palmitate/oleate ($P < 0.001$; Fig. 6a). To test the rejuvenating effect of exogenous fatty acids in the context of myogenesis, we performed a transplantation experiment in which we exposed old (24 month) MuSCs to 200 µM palmitate/oleate after isolation to support activation before transplantation into injured, 24-month-old recipients (Fig. 6b). The palmitate/oleate-treated MuSCs formed myofibers that were, on average, 417 um^2 larger (approximately 45%) than contralateral limb BSA (vehicle)-treated fibers ($P = 0.019$; Fig. 6c,d) and had 220% greater engraftment rates ($P = 0.011$; Fig. 6e). Furthermore, we tested to see if these results extended to a physiological, functional recovery of the hindlimbs using this metabolite replacement approach. We performed three assessments of mouse physical function at baseline and 14 days after the same injury/transplantation shown in Fig. 6b with outcomes similar to Kang et al.[19], including RotaRod performance test, open-field activity monitoring and treadmill gate analysis of hindlimbs. Twenty-four-month-old mice receiving palmitate/oleate-treated MuSCs had physical function closer to the uninjured state when assessed 14 days after injury by RotaRod (Fig. 6f; $P = 0.024$), open-field activity monitoring (Fig. 6g; $P = 0.044$) and hindlimb gait analysis (Fig. 6h; $P = 0.017$ for brake phase, $P = 0.011$ for propel phase). These results support our hypothesis that aged MuSCs have a reduced capacity for reductive glutamine metabolism and downstream DNL. By restoring the fatty acyl end product, aged MuSC returns proliferative, myogenic function and hindlimb functional recovery.

https://doi.org/10.1038/s43587-026-01120-3

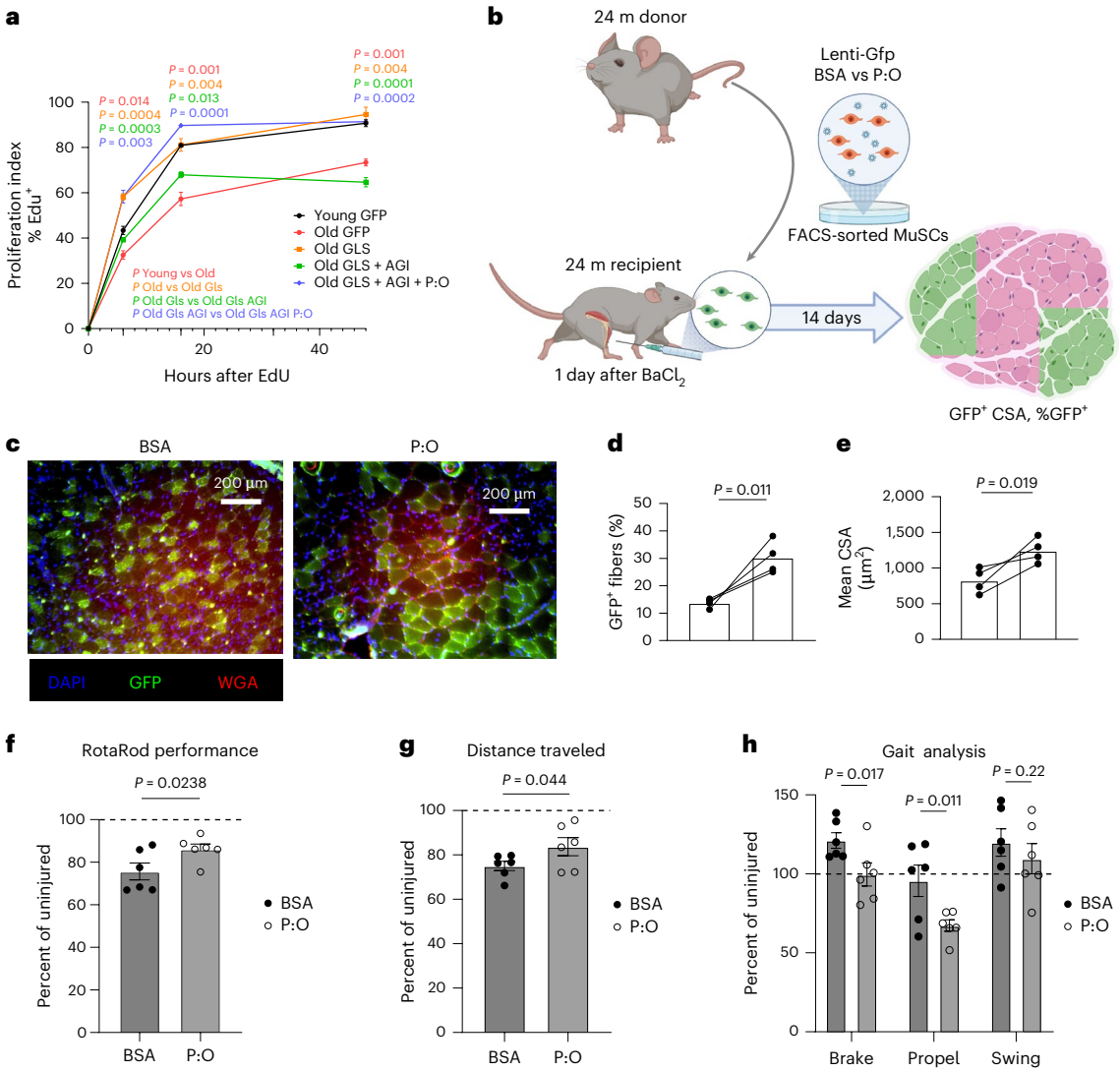


Fig. 6 | Reductive glutamine flux supports MuSC activation via DNL. a, EdU incorporation timecourse of MuSCs from 6-month and 24-month wild-type mice transduced with GFP or GLS lentivirus and combining AGI678 inhibitor treatment with exogenous palmitate:oleate (P:O) ($n = 3$ biological replicates per group; data are mean ± s.e.m.). **b**–**e**, Experimental design (**b**), micrographs (**c**) and quantification of MuSC transplant experiment in 24-month-old mice using MuSCs treated with P:O (**d**,**e**) (data are mean ± s.e.m.; *P* value indicates one-tailed *t*-test). Connected datapoints in **d** and **e** are matching samples from the same mouse ($n = 4$ recipient mice). **f**–**h**, Functional recovery of mouse hindlimbs from experiments in **b** was measured by RotaRod (**f**), open-field activity (**g**) and hindlimb gait analysis (**h**). **f**–**h**, *P* values indicate one-tailed *t*-tests; numbers are shown as percent of the uninjured measurement (indicated by dashed line at 100) ($n = 6$ per group; data are mean ± s.e.m.). m, month. Graphic in **b** created in BioRender; Lee, D. https://biorender.com/5jy97i9 (2026).

Discussion

MuSC function is recognized as a critical process for successful maintenance and regeneration of skeletal muscle[5]. Understanding metabolic adaptations that occur in this cellular remodeling and proliferation process could present targets for therapeutic intervention to sustain MuSC regenerative function with age. In this study, we identify glutamine metabolism by GLS to be necessary for MuSC function. We extend these observations by showing that GLS is required for both oxidative energy production and reductive counterclockwise TCA metabolism. Aged MuSCs have reduced capacity to metabolize glutamine due to the reduction in GLS abundance. When GLS function is restored in the aged MuSC, proliferative function returns, which is dependent on reductive flux through the TCA cycle. Lastly, we use targeted metabolomics and metabolic flux analyses to demonstrate that reductive glutamine metabolism in the TCA cycle supports DNL as a key pathway for MuSC activation and cellular proliferation. Collectively, these data identify a supportive role of glutamine metabolism in the MuSC and potential therapeutic targets to restore stem cell function with age, including a reductive pathway required for MuSC energy production, biosynthetic pathways and function.

Traditional glutamine metabolic circuits lead to production of glutamate and α-ketoglutarate for oxidation of the latter in the TCA cycle as well as other metabolic pathways, including serine biosynthesis[20,21]. Reductive metabolism of glutamine in the TCA cycle has been shown to be active in cancer models[22] as well as metabolic control of insulin secretion from pancreatic islet β cells, demonstrating that this metabolic pathway is not unique to cancer cells and can contribute to non-pathological cellular functions[16]. Supporting this idea, we were able to demonstrate that GLS activity is required for normal MuSC activation in vitro, in situ and in vivo. We also found that glutamine is metabolized in MuSCs by both oxidative and reductive pathways, each contributing to stem cell activation and proliferation. Our data agree with those recently published by Soro-Arnáiz et al.[12], which also measured reductive TCA carboxylation of glutamine in proliferating

myoblasts, which drops off significantly in differentiated myotubes. We sought to further elucidate the downstream metabolic outcomes of this cell-state-specific metabolic activity, especially in the context of aging.

Satellite cells exhibit unique cycles of quiescence and activation to contribute to myonuclear accretion without exhausting the MuSC pool. In the quiescent (or G_0) state, MuSCs have relatively small cytoplasm and limited stores of amino acids, lipids and other metabolic substrates. Once a satellite cell is stimulated to enter the cell cycle, a conserved stress response begins to coordinate transcriptional changes to drive protein synthesis, nucleotide synthesis and ATP production in preparation for the initial cell replication event (typically within 40 hours of activation)[23,24]. Additionally, the satellite cell niche maintains MuSCs in a state of relative hypoxia to limit oxidation of metabolic fuels[25–27]. These unique characteristics of the MuSC underscore the need for metabolic flexibility to support successful activation. Examples of this include the uptake of macrophage-derived glutamine[28] and the generation of ATP via autophagy stimulation[6]. Our results define a non-canonical metabolic pathway supporting stem cell activation, the IDH2-driven reductive metabolism of glutamine in the TCA cycle. As originally described in oncogenic hepatocytes, the reverse shunting of glutamine through the TCA cycle yields NADPH and citrate, both of which support DNL[22]. Synthesis of fatty acids by DNL in rapidly proliferating or differentiating cells provides precursors for synthesis of triglyceride, phospholipids and other complex lipids necessary for membrane biogenesis. Our data clearly demonstrate the activation of these pathways in activating MuSCs using metabolic flux analysis to measure glutamine flux and DNL.

Natural aging can present with a plethora of muscle-related ailments, including decreased ambulation, muscle mass and regenerative capacity as well as MuSC exhaustion[2]. Maintaining the pool of MuSCs and their ability to successfully activate may help prevent sarcopenia while enhancing physical capacity and socioeconomic productivity in aging populations[29]. We identified GLS as an enzyme contributing to the loss of oxidative capacity during MuSC activation in aging and potentially implicating GLS activity in the maintenance of the PAX7 satellite cell pool via self-renewal (Fig. 2o–q). Furthermore, we showed that restoration of GLS in MuSCs can rescue oxidative capacity and MuSC activation while also enhancing regeneration, as shown by our transplantation studies in old, sarcopenic mice. Data from other groups do support the age-related downregulation of *Gls1* at the transcriptional level[15] despite little change to the chromatin accessibility surrounding the *Gls1* coding sequence[30]. Evidence from caloric restrictions[31], AMPK[9,32], rapamycin[33], FoxO[34] and SIRT1 (ref. 7) transgenic studies show that improving metabolic flexibility in aged MuSCs can improve regenerative function. These studies highlighted changes in mitochondrial dynamics during MuSC activation, including markers of mitochondrial biogenesis and increased OCRs. Our results build upon and extend this foundational knowledge by demonstrating that MuSCs exhibit age-dependent differences in reductive glutamine flux. Moreover, when we blocked reductive TCA flux using AGI6780, we saw an increase in oxygen consumption (glutamine flux is forced toward oxidation) concomitant with signs of mitochondrial uncoupling (oligomycin-resistant oxygen consumption (Figs. 4i and 5e) and a shift away from an energized nucleotide profile in Fig. 5c). There is precedent for transient UCP2 expression in myoblasts during proliferation and differentiation[35–37]. Taken together, this suggests that MuSC activation requires controlled oxidative TCA cycle flux for cellular remodeling and mitigating excessive redox stress. Our experiments did not test the necessity of glutamine metabolism for rapamycin or calorie restriction-mediated rejuvenation effects on MuSCs; however, we do provide evidence that directly replacing the downstream metabolic products of glutamine-fueled reductive flux and DNL (palmitate/oleate in this case) is sufficient to produce similar functional benefits (in vitro activation and transplantation) as the GLS enzyme itself (Fig. 5). Future studies should identify terminal metabolic products that might be replenished to offer metabolic support during MuSC activation; analyze complex lipids to understand changes in the lipidomic landscape during activation and supported by glutamine reductive TCA flux; and endeavor to further understand the small-molecule metabolite dynamics in and around the MuSC niche, especially during regeneration.

In summary, we identify GLS-driven reductive TCA flux in the MuSC as a key metabolic pathway supporting DNL during MuSC activation. Leveraging static and flux approaches to stem cell metabolomics, we identified several unique metabolic characteristics of the activating MuSC at the level of specific metabolic pathways and small-molecule metabolite levels rather than the more global transcriptomic or protein level. Age-related detriments to these pathways may account for lost function and exhaustion of the MuSC pool. Moreover, replenishing GLS or downstream metabolites such as palmitate may serve as new strategies for achieving functional rejuvenation of MuSC function.

Methods

Animals

All animal experiments and care followed the guidelines of, and were approved by, the Institutional Animal Care and Use Committee at Duke University Medical Center (protocol A027-24-01). For experiments with wild-type mice, male C57/BL6J mice were acquired through the National Institute on Aging animal colony and used for experiments at 6–8 months of age (labeled as 'young') or at age 24–26 months (labeled as 'old'). The *Pax7*-CreER^{T2} mouse was acquired through The Jackson Laboratory (Gaka strain, ID: 017763). *Gls*$^{fl/fl}$ mice were a kind gift from C. Karner and are available through The Jackson Laboratory (ID: 017894). The GFP mice used were acquired from The Jackson Laboratory (*ACTB*-GFP, ID: 006567). All mice were housed in a climate-controlled facility with temperature maintained at 22°C ± −1°C, humidity maintained between 30% and 70% and a 12-hour light/dark cycle with water and chow (PMI 5053, Picolab Rodent Diet 20) available ad libidum. Once experimental endpoints were reached, mice were euthanized by CO_2 asphyxiation for >5 minutes followed by decapitation.

Muscle injury

$BaCl_2$ was used to induce muscle damage in tibialis anterior muscle via intramuscular injection of 30 µl of 1.2% (v/v) $BaCl_2$ in PBS using a 30-gauge needle. Control muscles were injected with an equal volume of PBS.

Primary mouse MuSC isolation by FACS

Mouse muscles were processed into a single-cell suspension for flow cytometry or FACS using methods adapted from Liu et al.[38]. Triceps, quadriceps, hamstrings, tibialis anterior, gastrocnemius, soleus and plantaris muscles were collected from uninjured mice, or tibialis anterior muscles were used in mouse injury experiments. Muscles were dissected, minced using scissors, digested in 10 ml of F10 + 10% (v/v) horse serum and 1,000 U ml^{-1} Collagenase II (Worthington Biochemical) for 60 minutes at 37 C in a shaking water bath, washed in F10 media, digested again for 30 minutes at 37 C in F10 + 10% (v/v) horse serum + 1.1 U ml^{-1} dispase (Gibco) and 100 U ml^{-1} Collagenase II, washed, passed through a 40-µm cell strainer and stained with antibodies for flow cytometry. Cells were identified on flow cytometers by forward scatter and side scatter parameters. For MuSC isolation, cells were negatively gated for APC-CD45, APC-CD11b, APC-Ter119 and APC-CD31 and FITC-SCA1 populations before selecting VCAM$^+$ cells. Flow cytometry and FACS were performed on a Sony SH800 cell sorter equipped with four lasers and appropriate detector filter sets. Cell sorting was performed in a biosafety cabinet at 4 °C using a 100-µm microfluidic chip at a pressure near 20 PSI. Cells were collected in media used for culturing but washed once prior to seeding to remove FACS sorting sheath fluid. After sorting, analysis was routinely used to confirm successful sorter calibration. For isolation of VCAM1$^+$ MuSCs from GFP mouse muscle, identical methods were used with the exception of the FITC-SCA1 antibody, which was replaced with APC-SCA1 (Supplementary Fig. 7).

MuSC culture and in vitro analysis

Isolated MuSCs were collected by FACS and cultured on tissue culture-treated plates (384-well, 48-well, 12-well and Seahorse XFe24), which were pretreated with 1 μg ml^{-1} collagen and 5 μg ml^{-1} laminin in PBS for at least 2 hours. Culture medium for proliferation, TUNEL and Seahorse assays was F10 supplemented with 10% horse serum, 10% FBS, 1% penicillin–streptomycin and 10 ng ml^{-1} bFGF (Gibco, 13256-029). For isotope labeling studies, culture media were changed to DMEM without glucose, pyruvate, glutamine or phenol red (Gibco, A1443001) and supplemented with 10% horse serum, 10% FBS, 1% penicillin–streptomycin and 10 ng ml^{-1} bFGF for a 10-minute washout before replacing with the same DMEM mixture with 1 M glucose and 200 μM glutamine (either $^{12}C_5$ for negative control or $^{13}C_5$ for isotope labeling (Sigma-Aldrich, 605166)). For lentiviral isotope labeling study (Supplementary Fig. 4), the labeling media were modified to contain no glucose for maximal stimulation of TCA metabolism of glutamine. For EdU labeling, 10 μM EdU was added to culture media at the time of seeding isolated MuSCs and fixed using 10% formalin for 10 minutes at the times indicated. EdU was visualized using Click-&-Go Imaging Kit (Click Chemistry Tools, 1314). TUNEL analysis was performed on MuSCs fixed 24 hours after isolation using TUNEL assay kit (Abcam, ab66108). Seahorse Extracellular Flux analysis was performed on Seahorse XFe24 platform according to manufacturer protocols and using drug concentrations previously published and optimized[39,40]. Rate data were normalized to total cell number or protein mass, which was quantified immediately after the analysis. For studies where MuSCs were supplemented with exogenous fatty acids, we supplemented media with 200 μM palmitate/oleate conjugated to BSA at a 1:1 ratio as previously optimized[17]. Our previous studies support the inclusion of both oleate alongside palmitate to provide a physiological blend of fatty acyls to the cells[17,18].

Single myofiber isolation and culture

After euthanasia, the extensor digitorum longus muscle was carefully dissected to avoid shearing or tearing and placed in 0.5% Collagenase I (Worthington Biochemical) in DMEM at 37 °C for 90 minutes. After three washes in DMEM, individual fibers were triturated with flame-polished glass pipettes for approximately 3–5 minutes to release myofibers. After a 60-minute equilibration period, intact, individual fibers were selected and transferred to an ECM-coated 24-well culture dish and cultured until experimental endpoints in DMEM containing 1% penicillin–streptomycin, 10% FBS and 1% chicken embryo extract. After 72 hours, myofibers were gently rinsed in two changes of 10% formalin for 10 minutes to fix samples before immunofluorescence staining.

LC–MS-based metabolomics of isolated MuSCs

For metabolomics analyses summarized in Fig. 1, MuSCs were isolated by FACS and seeded at approximtely 100,000 cells per well of a 12-well dish. Cells were cultured/activated for 24 hours, rinsed with deionized water, covered in ice-cold 80% methanol/20% water (v/v) for 10 minutes on dry ice to extract metabolites, centrifuged at 18,000*g* for 10 minutes to remove debris and dried under vacuum centrifugation. Extracts were reconstituted in liquid chromatography solvent for hydrophilic interaction chromatography (HILIC) and analyzed with an Agilent Infinity II 1290 UHPLC coupled to an Agilent 6546 Q-TOF mass spectrometer. Chromatography gradient parameters were set to a flow rate of 0.350 ml min^{-1}, progressing from 10% to 60% mobile phase B. Mass scanning was performed from 50 *m*/*z* to 1,200 *m*/*z*. Metabolite peaks were matched and quantified to in-house standard library using retention time and *m*/*z* matching using Agilent Profinder software version 10.0. Compound isotope peaks were extracted, integrated and corrected to background abundances. Values were normalized as a percent abundance of the total abundance of all isotopes of that metabolite.

Muscle histology

Muscle architecture was analyzed using OCT-embedded tibialis anterior muscles which were frozen in liquid nitrogen-cooled isopentane. Then, 10-μm cross-sections were cut using a cryotome and stained using H&E or immunofluorescence staining of eMHC. Images were taken using an Olympus microscope and analyzed using ImageJ software to determine area of individual fibers and number of GFP fibers. CSA was calculated by determining area of >100 fibers across three images for each sample and using this result to average with each sample from that experimental group. For immunofluorescence imaging (myofibers, eMHC and GFP transplants), slides were incubated in 10% formalin for 20 minutes and 0.1 M glycine for 10 minutes and blocked/permeabilized in 5% goat serum, 2% BSA, 0.1% Triton X-100 in PBS for 1 hour at room temperature before antibody staining. All images were taken using identical camera and light settings. All image quantification was done blinded to experimental group. To analyze interstitial versus subsarcolemmal MuSCs in PAX7/laminin co-stained sections, we used reference (wild-type uninjured) images to exemplify quiescent (subsarcolemmal) nuclei, which were typically nearer the spaces between fibers and showed clear overlap with laminin, whereas interstitial nuclei were identified by less overlap with laminin or overlapping with fiber regions.

MuSC transplantation

For MuSC transplantation, donor mouse muscle was dissected, and MuSCs were isolated as described above. When MuSCs were cultured, 1×10^7 lentiviral open reading frame (ORF) mGFP or lenti-ORF Gls1 particles were added to 20,000 cells in culture. After 24 hours, GFP fluorescence was confirmed and cells were trypsinized, rinsed in PBS with 5% FBS and injected into recipient mouse tibialis anterior muscles. Recipient mice were syngeneic young (6–8 months) or old (24 months) and were injected with $BaCl_2$ to induce muscle damage 24 hours prior to transplantation. Recipient mice were euthanized, and tibialis anterior muscles were snap frozen for histology of GFP$^+$ fibers 14 days after $BaCl_2$-induced injury (that is, 13 days after transplantation). Histology images were analyzed for GFP$^+$ fiber number and GFP fiber CSA. Where indicated, fatty acid synthase inhibitor and palmitic acid solution were included in the culture media of donor MuSCs during the 24-hour lentiviral labeling period. Fatty acid synthase inhibitor (Sigma-Aldrich, GSK2194069, referred to as FASNi) was used at a concentration of 20 nM with DMSO vehicle as control. Fatty acid supplementation used 100 μM palmitate/100 μM oleate conjugated to fatty acid-depleted BSA at 7% BSA and supplemented to culture media with unconjugated BSA as control.

Stable isotope tracer flux analysis

MuSCs were isolated by FACS from young and old mouse muscles. In total, 200,000 cells were cultured in 12-well dishes for 16 hours before media were rinsed and replaced by media lacking unlabeled glutamine and with 200 μM L-glutamine-$^{13}C_5$ (U-^{13}C glutamine; Sigma-Aldrich, 605166) substituted (see the 'MuSC culture and in vitro analysis' section for details). After 2 hours of labeling, cells were washed with ice-cold PBS and scraped in 1 ml of ice-cold methanol. Debris was pelleted, and cell extracts were dried by vacuum centrifugation. Dried residues were derivatized by resuspending in 25 μl of methoxylamine hydrochloride (2% w/v in pyridine) and incubated for 90 minutes at 40 °C followed by addition of 25 μl of MTBSTFA + 1% TBDMS and incubation at 60 °C for 30 minutes. Samples were transferred to GC–MS autosampler vials and analyzed using an Agilent 7890B GC system equipped with HP-5MS capillary column (30 m, 0.25 mm ID, 0.25-μm phase thickness; Agilent J&W Scientific) operating at 80 °C for 2 minutes and increasing to 280 °C at 7 °C per minute for a total run time of 40 minutes. This was connected to an Agilent 5977A mass spectrometer operating under ionization by electron impact at 70 eV. Helium flow was maintained at 1 ml min^{-1}. Source temperature was maintained at 230 °C, the mass spectrometry

quad temperature at 150 °C, interface temperature at 280 °C and inlet at 250 °C. Mass spectra were recorded in mass scan mode with m/z range of 50–700. After identification of individual metabolites, the distribution of isotopologue labeling was determined and quantified in MassProfiler software. For each experiment, three biological replicates per group (cells isolated from separate animals) were pooled and analyzed across three separate isolation experiments. All samples from separate isolations were analyzed by GC–MS in the same batch.

For DNL studies, approximately 5×10^6 freshly isolated MuSCs were cultured in 10-cm dishes, and, approximately 12 hours after isolation, media were replaced with labeling medium consisting of culture medium supplemented with 6% ^2H_2O for 24 hours to allow labeling of newly synthesized fatty acids. Methanol extracts of cells were harvested, dried, hydrolyzed at 85 °C for 30 minutes and acidified with 6 M HCl before chloroform extraction of fatty acids for derivatization. GC–MS analysis was performed on the same instrumentation setup as detailed above. M0 palmitate (m/z 313) was used as unlabeled reference standard with other isotopomers quantified and normalized to total palmitate and cell number to quantify DNL[16,41,42].

For validation studies of inhibitors (Supplementary Figs. 2 and 6), identical labeling protocols were used for glutamine flux analysis applied to proliferating C2C12 myoblasts. Similar proportions of TCA intermediates were labeled by $^{13}C_5$-glutamine in C2C12 myoblasts as primary mouse MuSC (Fig. 4b–e and Supplementary Fig. 2a), supporting their use for metabolic inhibitor validation studies. C2C12 cells were acquired through the American Type Culture Collection (line CRL-1772).

Targeted metabolomics analysis of MuSCs

For experiments performed in Fig. 5, MuSCs were FACS isolated and cultured for 24 hours with DMSO or 10 µM AGI6780 (Sigma-Aldrich, SML0895) before extracts were collected as described for non-targeted metabolomics. For analysis of fatty acids and amino acids, samples were derivatized and analyzed by the same GC–MS approach as detailed for isotope tracer studies with the inclusion of deuterated myristic acid as internal standard. Using the standard, spectra were annotated to metabolites using an in-house, retention time-locked standard library and quantified by peak area[43–45]. For nucleotide analysis, samples were analyzed using Waters Xevo TQ-XS quadrupole mass spectrometry coupled to Acquity UPLC system and Chromolity FastGradient RP-18e 50 × 2-mm column (EMD Millipore). Nucleotides were detected in negative ion multiple reaction monitoring mode based on characteristic fragmentation reactions[46].

Antibodies

Antibodies used included the following: APC anti-mouse CD45 (1:200; BioLegend, 157605), APC anti-mouse CD11b (1:200; BioLegend, 101211), PE anti-mouse CD106 (1:50, VCAM; BioLegend, 105713), FITC anti-mouse Ly6A/E (1:40, SCA1; BioLegend, 108105), APC anti-mouse Ly6A/E (1:50, SCA1; BioLegend, 163806), Pacific Blue Annexin V (BioLegend, 640926) and rabbit anti-glutaminase 1 (1:500; Cell Signaling Technology, 88964). For immunofluorescence, mouse-PAX7 (supernatant used at 1:50; Developmental Studies Hybridoma Bank, AB_528428), rabbit-Ki67 (1:1,000; Abcam, ab15580), rabbit-laminin (1:500; Sigma-Aldrich, L9393) and mouse-eMHC (1:500; Developmental Studies Hybridoma Bank, F1.652) were used with DAPI and Phalloidin-TRITC (Sigma-Aldrich, P1951) used to visualize nuclei and actin filaments.

Hindlimb functional analysis

Mice were subjected to three assessments to gauge recovery of hindlimb functional capacity after $BaCl_2$ injury: RotaRod (Scantox), open-field cage activity and hindlimb gait analysis. Mice were acclimated/familiarized with testing procedures 3 days prior to a baseline assessment. After baseline assessment, mice were subjected to $BaCl_2$ muscle injury and MuSC transplantation as detailed above. Fourteen days after $BaCl_2$ injury, follow-up assessments were performed to gauge recovery. Results were calculated as a percent of baseline measurement. For RotaRod, mice were balanced on a rotating rod that began at 4 r.p.m. and accelerated to 40 r.p.m. over 300 seconds and were assessed as latency to fall in seconds. Five repeated tests were performed with the best and worst performance excluded. For open-field cage activity, mice were allowed free exploration of a 20 × 20 × 30-cm open-field arena for 15 minutes with video tracking to analyze voluntary movement measured as distance traveled in centimeters. For TreadScan Gait Analysis (Clever Sys), mice were placed on a transparent treadmill moving at 10 cm s^{-1} with video recording to determine foot swing and stance times. Only rear feet were analyzed (due to hindlimb injury protocol), and the side with the greatest change over the uninjured state (indicating decreased performance and, therefore, successful injury) was used to determine paw swing time, propel time and brake time averaged across 20 seconds of walking. Illustration of gait phases is presented in Fig. 6i of Kang et al.[19].

Statistical analysis

Statistical analyses performed included Student's t-test (unpaired and paired, one-tailed and two-tailed based on experimental design and hypothesis) between preplanned comparisons of two groups. All bar graphs presented are mean ± s.e.m., and α was set at $P < 0.05$. Hierarchical clustering heatmaps were generated in GraphPad Prism version 9. The number of replicates, statistical approach used as well as defined markers for significant comparisons or P values for each experiment are indicated in respective figure legends. For all cell culture experiments, technical replicates are not included in n values; instead, biological replicates (separate mice/isolations) are indicated and shown. For mass spectrometry studies (metabolomics), repeated measurements/mass spectrometer injections were averaged and used as resulting data for each biological sample, which are indicated by n values. Data distribution was assumed to be normal, but this was not formally tested. No statistical methods were used to predetermine sample sizes, but our sample sizes are similar to those reported in previous publications[47–50]. For all data quantifications (peak picking and micrograph counting/quantification), data processes were automated irrespective of sample grouping, or individuals performing processing were blinded to experimental group/condition. Animals were not randomly assigned to condition (young versus old, wild-type versus transgenic), but animals were randomly selected from within those predetermined groups for experiments, and each experiment was blocked such that all groups were represented.

Reporting summary

Further information on research design is available in the Nature Portfolio Reporting Summary linked to this article.

Data availability

All source data will be provided as a Source Data file. Other data will be available from the corresponding author upon reasonable request.

References

1. Martinez, B. P. et al. Frequency of sarcopenia and associated factors among hospitalized elderly patients. *BMC Musculoskelet. Disord.* **16**, 108 (2015).
2. Janssen, I., Shepard, D. S., Katzmarzyk, P. T. & Roubenoff, R. The healthcare costs of sarcopenia in the United States. *J. Am. Geriatr. Soc.* **52**, 80–85 (2004).
3. Masschelein, E. et al. Exercise promotes satellite cell contribution to myofibers in a load-dependent manner. *Skelet. Muscle* **10**, 21 (2020).
4. Folmes, C. D., Dzeja, P. P., Nelson, T. J. & Terzic, A. Metabolic plasticity in stem cell homeostasis and differentiation. *Cell Stem Cell* **11**, 596–606 (2012).

5. Pala, F. et al. Distinct metabolic states govern skeletal muscle stem cell fates during prenatal and postnatal myogenesis. *J. Cell Sci.* **131**, jcs212977 (2018).
6. Tang, A. H. & Rando, T. A. Induction of autophagy supports the bioenergetic demands of quiescent muscle stem cell activation. *EMBO J.* **33**, 2782–2797 (2014).
7. Ryall, J. G. et al. The NAD^+-dependent SIRT1 deacetylase translates a metabolic switch into regulatory epigenetics in skeletal muscle stem cells. *Cell Stem Cell* **16**, 171–183 (2015).
8. White, J. P. et al. The AMPK/$p27^{Kip1}$ axis regulates autophagy/apoptosis decisions in aged skeletal muscle stem cells. *Stem Cell Rep.* **11**, 425–439 (2018).
9. Theret, M. et al. AMPKα1-LDH pathway regulates muscle stem cell self-renewal by controlling metabolic homeostasis. *EMBO J.***36**, 1946–1962 (2017).
10. Yoo, H. C., Yu, Y. C., Sung, Y. & Han, J. M. Glutamine reliance in cell metabolism. *Exp. Mol. Med.* **52**, 1496–1516 (2020).
11. Yu, Y. et al. Glutamine metabolism regulates proliferation and lineage allocation in skeletal stem cells. *Cell Metab.* **29**, 966–978 (2019).
12. Soro-Arnáiz, I. et al. GLUD1 determines murine muscle stem cell fate by controlling mitochondrial glutamate levels. *Dev. Cell* **59**, 2850–2865 (2024).
13. Mullen, A. R. et al. Reductive carboxylation supports growth in tumour cells with defective mitochondria. *Nature* **481**, 385–388 (2011).
14. Mademtzoglou, D., Geara, P., Mourikis, P. & Relaix, F. Pax7 haploinsufficiency impairs muscle stem cell function in Cre-recombinase mice and underscores the importance of appropriate controls. *Stem Cell Res. Ther.* **14**, 294 (2023).
15. Lai, Y. et al. Multimodal cell atlas of the ageing human skeletal muscle. *Nature* **629**, 154–164 (2024).
16. Zhang, G. F. et al. Reductive TCA cycle metabolism fuels glutamine- and glucose-stimulated insulin secretion. *Cell Metab.* **33**, 804–817 (2021).
17. Koves, T. R. et al. Mitochondrial overload and incomplete fatty acid oxidation contribute to skeletal muscle insulin resistance. *Cell Metab.* **7**, 45–56 (2008).
18. Seiler, S. E. et al. Obesity and lipid stress inhibit carnitine acetyltransferase activity. *J. Lipid Res.* **55**, 635–644 (2014).
19. Kang, J. et al. Depletion of SAM leading to loss of heterochromatin drives muscle stem cell ageing. *Nat Metab.* **6**, 153–168 (2024).
20. Ciuffoli, V. et al. Psat1-generated α-ketoglutarate and glutamine promote muscle stem cell activation and regeneration. *Genes Dev.* **38**, 151–167 (2024).
21. Castegna, A. & Menga, A. Glutamine synthetase: localization dictates outcome. *Genes (Basel)* **9**, 108 (2018).
22. Holleran, A. L., Briscoe, D. A., Fiskum, G. & Kelleher, J. K. Glutamine metabolism in AS-30D hepatoma cells. Evidence for its conversion into lipids via reductive carboxylation. *Mol. Cell. Biochem.* **152**, 95–101 (1995).
23. Machado, L. et al. Tissue damage induces a conserved stress response that initiates quiescent muscle stem cell activation. *Cell Stem Cell* **28**, 1125–1135 (2021).
24. van Velthoven, C. T. J., de Morree, A., Egner, I. M., Brett, J. O. & Rando, T. A. Transcriptional profiling of quiescent muscle stem cells in vivo. *Cell Rep.* **21**, 1994–2004 (2017).
25. Urbani, L., Piccoli, M., Franzin, C., Pozzobon, M. & De Coppi, P. Hypoxia increases mouse satellite cell clone proliferation maintaining both in vitro and in vivo heterogeneity and myogenic potential. *PLoS ONE* **7**, e49860 (2012).
26. Liu, W. et al. Hypoxia promotes satellite cell self-renewal and enhances the efficiency of myoblast transplantation. *Development* **139**, 2857–2865 (2012).
27. Xie, L. et al. Transient HIF2A inhibition promotes satellite cell proliferation and muscle regeneration. *J. Clin. Invest.* **128**, 2339–2355 (2018).
28. Shang, M. et al. Macrophage-derived glutamine boosts satellite cells and muscle regeneration. *Nature* **587**, 626–631 (2020).
29. Brack, A. S. et al. Increased Wnt signaling during aging alters muscle stem cell fate and increases fibrosis. *Science***317**, 807–810 (2007).
30. Lazure, F. et al. Transcriptional reprogramming of skeletal muscle stem cells by the niche environment. *Nat. Commun.* **14**, 535 (2023).
31. Cerletti, M., Jang, Y. C., Finley, L. W., Haigis, M. C. & Wagers, A. J. Short-term calorie restriction enhances skeletal muscle stem cell function. *Cell Stem Cell* **10**, 515–519 (2012).
32. Kneppers, A. et al. AMPKα2 is a skeletal muscle stem cell intrinsic regulator of myonuclear accretion. *iScience* **26**, 108343 (2023).
33. García-Prat, L. et al. Autophagy maintains stemness by preventing senescence. *Nature* **529**, 37–42 (2016).
34. García-Prat, L. et al. FoxO maintains a genuine muscle stem-cell quiescent state until geriatric age. *Nat. Cell Biol.* **22**, 1307–1318 (2020).
35. Kim, D., Jitrapakdee, S. & Thompson, M. Differential regulation of the promoter activity of the mouse UCP2 and UCP3 genes by MyoD and myogenin. *J. Biochem. Mol. Biol.* **40**, 921–927 (2007).
36. Chen, X. et al. In vitro evidence suggests that miR-133a-mediated regulation of uncoupling protein 2 (UCP2) is an indispensable step in myogenic differentiation. *J. Biol. Chem.* **284**, 5362–5369 (2009).
37. McKellar, D. W. et al. Large-scale integration of single-cell transcriptomic data captures transitional progenitor states in mouse skeletal muscle regeneration. *Commun. Biol.* **4**, 1280 (2021).
38. Liu, L., Cheung, T. H., Charville, G. W. & Rando, T. A. Isolation of skeletal muscle stem cells by fluorescence-activated cell sorting. *Nat. Protoc.* **10**, 1612–1624 (2015).
39. Ly, C. H. & Ryall, J. G. Measuring mitochondrial substrate utilization in skeletal muscle stem cells. *Methods Mol. Biol.* **1668**, 61–73 (2017).
40. Yue, F. et al. Lipid droplet dynamics regulate adult muscle stem cell fate. *Cell Rep.* **38**, 110267 (2022).
41. White, P. J. et al. The BCKDH kinase and phosphatase integrate BCAA and lipid metabolism via regulation of ATP-citrate lyase. *Cell Metab.* **27**, 1281–1293 (2018).
42. Yenilmez, B. et al. Paradoxical activation of transcription factor SREBP1c and de novo lipogenesis by hepatocyte-selective ATP-citrate lyase depletion in obese mice. *J. Biol. Chem.* **298**, 102401 (2022).
43. Scholtens, D. M. et al. Metabolomics reveals broad-scale metabolic perturbations in hyperglycemic mothers during pregnancy. *Diabetes Care* **37**, 158–166 (2014).
44. Parry, T. L. et al. Untargeted metabolomics analysis of ischemia-reperfusion-injured hearts ex vivo from sedentary and exercise-trained rats. *Metabolomics* **14**, 8 (2018).
45. Liu, Y. et al. Metabolomic and genetic associations with insulin resistance in pregnancy. *Diabetologia* **63**, 1783–1795 (2020).
46. Gooding, J. R. et al. Adenylosuccinate is an insulin secretagogue derived from glucose-induced purine metabolism. *Cell Rep.* **13**, 157–167 (2015).
47. Baht, G. S. et al. Meteorin-like facilitates skeletal muscle repair through a Stat3/IGF-1 mechanism. *Nat. Metab.* **2**, 278–289 (2020).
48. Lee, D. E. et al. Meteorin-like is an injectable peptide that can enhance regeneration in aged muscle through immune-driven fibro/adipogenic progenitor signaling. *Nat. Commun.* **13**, 7613 (2022).
49. Lee, D. E. et al. Mitochondrial mRNA translation initiation contributes to oxidative metabolism in the myocardia of aged, obese mice. *Exp. Gerontol.* **121**, 62–70 (2019).

50. Lee, D. E. et al. Translational machinery of mitochondrial mRNA is promoted by physical activity in Western diet-induced obese mice. *Acta Physiol. (Oxf.)* **218**, 167–177 (2016).

Acknowledgements

This work was supported by the following awards: National Institutes of Health (NIH)/National Institute on Aging (NIA) grant K01AG056664 (J.P.W.), grant R21AG065943 (J.P.W.), NIH training grant T32HL007057 (D.E.L.), grant K01AG088232 (D.E.L.), Borden's Scholar Award (D.E.L.), NIH/National Institute of Dental and Craniofacial Research (NIDCR) grant K08DE031029 (L.K.M.), NIH/National Institute of Diabetes and Digestive and Kidney Diseases (NIDDK) grant R01DK132819 (S.K.), NIH grant DK046092 (C.B.N.) and Duke Aging Center/Pepper Center grant P30-AG028716 (J.R.B.). The metabolomic and metabolic flux analyses reported here were supported by funding from the North Carolina Diabetes Research Center NIDDK grant P30DK124723 (C.B.N.). The funders had no role in study design, data collection and analysis, decision to publish or preparation of the manuscript.

Author contributions

D.E.L., J.P.W., J.R.B., G.-F.Z. and C.B.N. conceived and/or designed experiments. D.E.L., L.K.M., A.B., W.H., D.H., J.R.B., J.Y., G.-F.Z. and S.K. acquired, analyzed and/or interpreted data. D.E.L., L.K.M. and J.P.W. drafted the paper. D.E.L. and J.P.W. revised the paper. All authors approved the final version.

Competing interests

C.B.N. is a paid consultant for Eli Lilly, Axcella Health, Boehringer Ingelheim and Sigilon, which were not involved and have no competing interest in the research described in this paper. The other authors declare no competing interests.

Additional information

Supplementary information The online version contains supplementary material available at https://doi.org/10.1038/s43587-026-01120-3.

Correspondence and requests for materials should be addressed to James P. White.

Peer review information *Nature Aging* thanks the anonymous, reviewer(s) for their contribution to the peer review of this work. Peer reviewer reports are available.

Reprints and permissions information is available at www.nature.com/reprints.

Publisher's note Springer Nature remains neutral with regard to jurisdictional claims in published maps and institutional affiliations.

Springer Nature or its licensor (e.g. a society or other partner) holds exclusive rights to this article under a publishing agreement with the author(s) or other rightsholder(s); author self-archiving of the accepted manuscript version of this article is solely governed by the terms of such publishing agreement and applicable law.

© The Author(s), under exclusive licence to Springer Nature America, Inc. 2026

nature portfolio

Corresponding author(s): James P. White

Last updated by author(s): 3/5/2026

Reporting Summary

Nature Portfolio wishes to improve the reproducibility of the work that we publish. This form provides structure for consistency and transparency in reporting. For further information on Nature Portfolio policies, see our Editorial Policies and the Editorial Policy Checklist.

Statistics

For all statistical analyses, confirm that the following items are present in the figure legend, table legend, main text, or Methods section.

n/a	Confirmed
☐	☒ The exact sample size (*n*) for each experimental group/condition, given as a discrete number and unit of measurement
☐	☒ A statement on whether measurements were taken from distinct samples or whether the same sample was measured repeatedly
☐	☒ The statistical test(s) used AND whether they are one- or two-sided *Only common tests should be described solely by name; describe more complex techniques in the Methods section.*
☐	☒ A description of all covariates tested
☐	☒ A description of any assumptions or corrections, such as tests of normality and adjustment for multiple comparisons
☐	☒ A full description of the statistical parameters including central tendency (e.g. means) or other basic estimates (e.g. regression coefficient) AND variation (e.g. standard deviation) or associated estimates of uncertainty (e.g. confidence intervals)
☐	☒ For null hypothesis testing, the test statistic (e.g. *F*, *t*, *r*) with confidence intervals, effect sizes, degrees of freedom and *P* value noted *Give P values as exact values whenever suitable.*
☒	☐ For Bayesian analysis, information on the choice of priors and Markov chain Monte Carlo settings
☒	☐ For hierarchical and complex designs, identification of the appropriate level for tests and full reporting of outcomes
☒	☐ Estimates of effect sizes (e.g. Cohen's *d*, Pearson's *r*), indicating how they were calculated

Our web collection on statistics for biologists contains articles on many of the points above.

Software and code

Policy information about availability of computer code

Data collection	ImageStudio V5.2 (LiCor Biosciences), MassHunter Acquisition V10.0 (agilent Technologies), Wave Desktop v2.6.4 (Seahorse, Agilent Technologies) Olympus CellSens standard Software v1.6.
Data analysis	FlowJo V 10.0 (BD), ImageJ 1.54(NIH), MassHunter Profinder V10.0 (Agilent), MassHunter Quant-my-way (GCMS) V10.0 (Agilent).

For manuscripts utilizing custom algorithms or software that are central to the research but not yet described in published literature, software must be made available to editors and reviewers. We strongly encourage code deposition in a community repository (e.g. GitHub). See the Nature Portfolio guidelines for submitting code & software for further information.

Data

Policy information about availability of data

All manuscripts must include a data availability statement. This statement should provide the following information, where applicable:

- Accession codes, unique identifiers, or web links for publicly available datasets
- A description of any restrictions on data availability
- For clinical datasets or third party data, please ensure that the statement adheres to our policy

All source data will be provided as source data file.

Research involving human participants, their data, or biological material

Policy information about studies with human participants or human data. See also policy information about sex, gender (identity/presentation), and sexual orientation and race, ethnicity and racism.

Reporting on sex and gender	No human participants were used in these studies.
Reporting on race, ethnicity, or other socially relevant groupings	*Please specify the socially constructed or socially relevant categorization variable(s) used in your manuscript and explain why they were used. Please note that such variables should not be used as proxies for other socially constructed/relevant variables (for example, race or ethnicity should not be used as a proxy for socioeconomic status).* *Provide clear definitions of the relevant terms used, how they were provided (by the participants/respondents, the researchers, or third parties), and the method(s) used to classify people into the different categories (e.g. self-report, census or administrative data, social media data, etc.)* *Please provide details about how you controlled for confounding variables in your analyses.*
Population characteristics	*Describe the covariate-relevant population characteristics of the human research participants (e.g. age, genotypic information, past and current diagnosis and treatment categories). If you filled out the behavioural & social sciences study design questions and have nothing to add here, write "See above."*
Recruitment	*Describe how participants were recruited. Outline any potential self-selection bias or other biases that may be present and how these are likely to impact results.*
Ethics oversight	*Identify the organization(s) that approved the study protocol.*

Note that full information on the approval of the study protocol must also be provided in the manuscript.

Field-specific reporting

Please select the one below that is the best fit for your research. If you are not sure, read the appropriate sections before making your selection.

☒ Life sciences ☐ Behavioural & social sciences ☐ Ecological, evolutionary & environmental sciences

For a reference copy of the document with all sections, see nature.com/documents/nr-reporting-summary-flat.pdf

Life sciences study design

All studies must disclose on these points even when the disclosure is negative.

Sample size	No a priori sample size/power calculations were included. Ex vivo experimental sample sizes were determined by the feasibility and throughput of stem cell collections through the isolation and FACS-sorting process (generally 8-12 mice/experiment max). For in vitro, transplantation and injury studies, we used similar sample sizes as we have previously published expecting similar effect sizes due to our independent variables: age (6months vs 24 months) and BaCl2 injury.
Data exclusions	For untargeted metabolomics experiments, if metabolite signal was absent, the data were not excluded but considered below detection. For statistical analysis, these data points were replaced with a value at 1/5 of the lowest detected value. For flux analysis, these were replaced with 0. If a metabolite had >50% missingness within an experimental group, the metabolite was excluded. These were pre-determined criteria.
Replication	The majority of cell culture studies could not be completed in a single experimental isolation; therefore, replicates were performed over several (usually 3) separate cell isolations with each experimental group being represented by each isolation. For some ex vivo studies (EdU, Seahorse) where several replicates of each group could be included in one isolation, multiple separate experiments were performed for replication. All attempts at replication that reached study endpoints were confirmed. In some replication attempts, cell isolations did not yield sufficient cell numbers and experiments were aborted.
Randomization	For cell isolation studies, samples were isolated and evenly distributed across experimental groups; therefore, no randomization was needed for ex vivo treatments. Animals were not randomized to biological groupings because these were predetermined by age or genotype. For transplantation analysis, contra lateral limb controls were used so no randomization of mice to groups was necessary.
Blinding	Investigators performing experiments (cell culture, cell transplantation) were not blinded to groups. All investigators were blinded to experimental group during data analysis (mass spectrometry peak analysis, microscopy image analysis, animal functional tests, etc.)

Reporting for specific materials, systems and methods

We require information from authors about some types of materials, experimental systems and methods used in many studies. Here, indicate whether each material, system or method listed is relevant to your study. If you are not sure if a list item applies to your research, read the appropriate section before selecting a response.

Materials & experimental systems

n/a	Involved in the study
☐	☒ Antibodies
☐	☒ Eukaryotic cell lines
☒	☐ Palaeontology and archaeology
☐	☒ Animals and other organisms
☒	☐ Clinical data
☒	☐ Dual use research of concern
☒	☐ Plants

Methods

n/a	Involved in the study
☒	☐ ChIP-seq
☐	☒ Flow cytometry
☒	☐ MRI-based neuroimaging

Antibodies

Antibodies used: Antibodies used included: APC anti-mouse CD45 (1:200, Biolegend 157605), APC anti-mouse CD11b (1:200, Biolegend, 101211), PE anti-mouse CD106 (1:50, VCAM, Biolegend 105713), FITC anti-mouse Ly6A/E (SCA1, 1:50, Biolegend, 108105), Pacific Blue AnnexinV (Biolegend 640926), rabbit anti-Glutaminase1 (1:500, Cell Signaling #88964). For immunofluorescence, mouse-PAX7 (1:50, DSHB AB_528428), Rabbit-Ki67 (1:1000, Abcam #ab15580), rabbit anti-laminin (Sigma #L9393,1:1000) and mouse-eMHC (1:500, DSHB F1.652)

Validation: No novel antibodies were developed or validated. All commercially available antibody validation data are available through the manufacturers.

Eukaryotic cell lines

Policy information about cell lines and Sex and Gender in Research

Cell line source(s): No primary cell experiments were preserved or passaged to generate a cell line. For validation studies in SFig 2,6, C2C12 mouse myoblasts were acquired from ATCC (CRL-1772) at Passage 0 and used before passage 5. C2C12 cells from ATCC CRL-1772 have not been identified as a contaminated cell ling by ICLAC

Authentication: We performed no authentication of C2C12 cells once acquired from ATCC.

Mycoplasma contamination: We performed no mycoplasma testing of C2C12 cells once acquired from ATCC.

Commonly misidentified lines (See ICLAC register): none

Animals and other research organisms

Policy information about studies involving animals; ARRIVE guidelines recommended for reporting animal research, and Sex and Gender in Research

Laboratory animals: Mus musculus, C56/B6J male mice were throughout these studies. Where indicated, young mice were used at ages between 6-8 months (post adolescent adulthood) and aged mice were used at 24-26months of age. Pax7CreERT2 and Gls1 fl/fl mice were either purchased through Jackson Laboratory (Gaka strain, Jax ID: 017763) or were gifted (see methods section for details). Both were on a C57B6 background strain. GFP experiments used were acquired from Jackson Laboratory (β-actin-GFP, strain id: 006567).

Wild animals: The study did not involve wild animals

Reporting on sex: The studies only apply to the sex used for each experiment (male). We do not report any sex-based comparisons.

Field-collected samples: The study did not involve field collected samples

Ethics oversight: The study was approved by the Duke University School of Medicine Institutional Animal Care and Use Committee.

Note that full information on the approval of the study protocol must also be provided in the manuscript.

Plants

Seed stocks: No plant material was used in these studies.

Novel plant genotypes: *Describe the methods by which all novel plant genotypes were produced. This includes those generated by transgenic approaches, gene editing, chemical/radiation-based mutagenesis and hybridization. For transgenic lines, describe the transformation method, the number of independent lines analyzed and the generation upon which experiments were performed. For gene-edited lines, describe the editor used, the endogenous sequence targeted for editing, the targeting guide RNA sequence (if applicable) and how the editor was applied.*

Authentication: *Describe any authentication procedures for each seed stock used or novel genotype generated. Describe any experiments used to assess the effect of a mutation and, where applicable, how potential secondary effects (e.g. second site T-DNA insertions, mosiacism, off-target gene editing) were examined.*

Flow Cytometry

Plots

Confirm that:

☒ The axis labels state the marker and fluorochrome used (e.g. CD4-FITC).

☒ The axis scales are clearly visible. Include numbers along axes only for bottom left plot of group (a 'group' is an analysis of identical markers).

☒ All plots are contour plots with outliers or pseudocolor plots.

☒ A numerical value for number of cells or percentage (with statistics) is provided.

Methodology

Sample preparation: cells were negatively gated for APC-CD45, APC-CD11b, APC-Ter119, and APC-CD31, and FITC-SCA1 populations before selecting VCAM+ cells. Flow cytometry and FACS were performed on Sony SH800 cell sorter equipped with 4 lasers and appropriate detector filter sets. Cell sorting was performed in biosafety cabinet at 4C using 100uM microfluidic chip at a pressure near 20PSI. Cells were collected in media used for culturing but washed once prior to seeding to remove FACS sorting sheath fluid. Post sorting analysis was routinely used to confirm successful sorter calibration.

Instrument: Sony SH800

Software: Sony Sorter software (data collection, sorting). FlowJo V 10 (data analysis, visualization

Cell population abundance: See Supplementary Figure 1. Post sort fraction validation was routinely tested at >90% pure and live.

Gating strategy: See Supplementary Figure 1. Cells were selected by FSC/SSC selection and gating. Dublets were excluded using FSC-HxFSC-A linearity (and gated from this). This population was negatively selected based on APC for several markers of hematopoietic cells (Cd11b, CD45, Ter119, CD31). This subpopulation was negatively selected for SCA1-FITC and positively selected based on VCAM1-PE for sorting.

☒ Tick this box to confirm that a figure exemplifying the gating strategy is provided in the Supplementary Information.